RGNZ/MGPB

# The effects of test specimen shape tolerances on determining the mechanical and energy dissipation properties of limestone rock

Rudarsko-geološko-naftni zbornik
(The Mining-Geology-Petroleum Engineering Bulletin)
DOI: 10.17794/rgn.2025.3.12

Original scientific paper

**Nataša Štambuk Cvitanović[1]*, Boris Kavur[2], Ivan Vrkljan[3], Predrag Miščević[1]**

[1] *University of Split, Faculty of Civil Engineering, Architecture and Geodesy, Matice hrvatske 15, Split, Croatia.*

[2] *University of Zagreb, Faculty of Geotechnical Engineering, Hallerova aleja 7, Varaždin, Croatia.*

[3] *University of Rijeka, Faculty of Civil Engineering, Radmile Matejčić 3, Rijeka, Croatia.*

**Abstract**

The uniaxial compressive strength (*UCS*), Young's modulus (*E*) and Poisson's ratio (*v*) of intact rock depend on the cylindrical specimen shape tolerances (flatness of ends *R*, their parallelism *P* and perpendicularity to the specimen axis *O*). Today's specimen acceptance criteria (allowable *R*/*P*/*O*) are based on scarce research data from the 1970s that mostly relate to *UCS* without considering the rock strength category (worst case scenario). They are also very strict and, in some cases, difficult to implement, requiring engineering judgment. To increase reliability and facilitate judgment of specimen acceptability, this study investigates the influence of shape tolerances on all *UCS*/*E*/*v* properties and related energy dissipation properties (total, elastic and dissipated energy) for limestone and comparable medium-strength rock with *UCS* around 100-150 MPa. Ninety specimens were prepared with target (wider) shape tolerances (*R* up to 0.5 mm; *P*, *O* up to 2°) using specially developed equipment for accurate *R*/*P*/*O* determination. These specimens were further tested in uniaxial compression with several relevant measurement settings and all mechanical and energy dissipation properties were determined. From many experimental results and additional statistical/numerical/energy analyses, reliable behaviour models for *UCS*/*E*/*v* dependence on *R*/*P*/*O* have been established that can be further used to assess the consequences of shape tolerances and specimen acceptability. If limits of natural variability for 'ideal' specimens are applied to these models, critical tolerances that reduce the existing requirements are obtained (e.g. *R* = 0.08 mm instead of 0.05 mm), which are proposed as supplementary to optimize the testing process for medium-strength rocks.

**Keywords:**

cylindrical rock test specimens, shape tolerances, mechanical properties, energy dissipation properties

## 1. Introduction

The mechanical properties of intact rock, such as strength and deformability, are fundamental in rock mechanics and geotechnical engineering projects. On the other hand, these properties – the uniaxial compressive strength *UCS*, Young's modulus *E*, and Poisson's ratio *v* – are influenced by the shape deviations of the test specimen (deviations from the ideal cylinder). These have not been sufficiently investigated, although their influence on the *UCS*/*E*/*v* can be significant (in the sense that shape deviations greater than a certain limit will result in lower strength and increased deformability). Namely, there is a noticeable diversity and inconsistency in the documents, standards and recommendations that address the acceptable shape deviation values of test specimens, so-called shape tolerances – side straightness, flatness and parallelism of the specimen ends and their perpendicularity to the specimen axis – as if there is no professional consensus on this issue. Certain requirements of the applicable standards, such as those of International Society for Rock Mechanics and Rock Engineering (ISRM) and ASTM (**ISRM, 1979; ASTM D4543-19, 2019**), are very difficult to meet for some rock types (weaker rock types, or more porous, from a jointed zone, poorly cemented, with significant or weak (or both) structural features). The reference values on which the criteria for acceptance or rejection of samples are based are very strict and date back to the 1970s (**Hoskins and Horino, 1968; Podnieks et al., 1972**).

In geotechnics, a small number of representative samples is often a significant problem, so the criteria for accepting/rejecting samples should receive adequate attention. In addition, the influence of shape tolerances on *UCS*/*E*/*v* is not equally pronounced for all types of rocks and all types of testing equipment, which also needs to be considered (**Štambuk Cvitanović, 2012; Štambuk Cvitanović et al., 2015a, 2015b; ASTM D4543-19, 2019**).

Following the strength and deformability tests on many samples over a long period in an accredited geo-

* Corresponding author: Nataša Štambuk Cvitanović
*e-mail address: nstambuk@gradst.hr*

Received: 10 January 2025. Accepted: 11 February 2025.
Available online: 3 July 2025

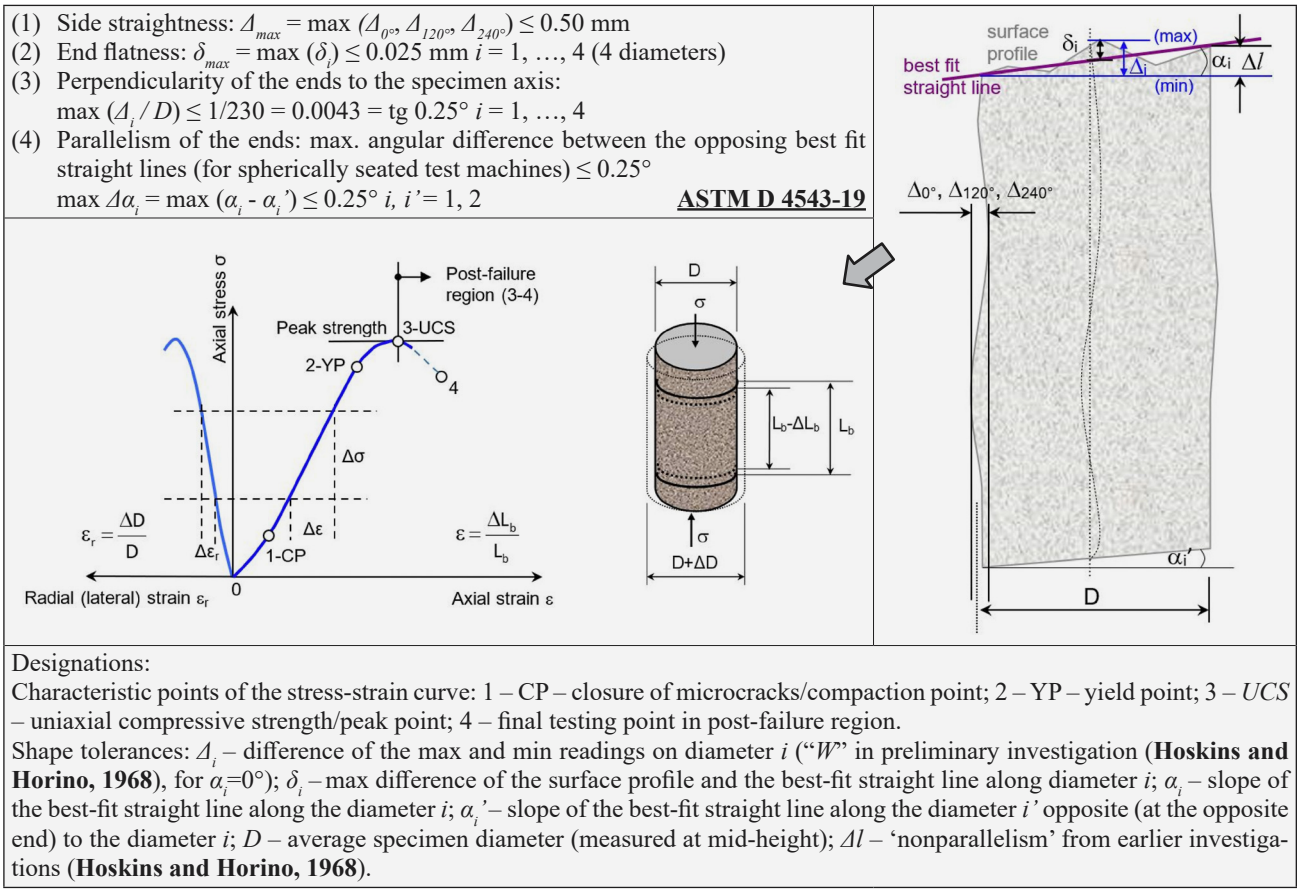


Designations:
Characteristic points of the stress-strain curve: 1 – CP – closure of microcracks/compaction point; 2 – YP – yield point; 3 – *UCS* – uniaxial compressive strength/peak point; 4 – final testing point in post-failure region.
Shape tolerances: $\Delta_i$ – difference of the max and min readings on diameter $i$ ("*W*" in preliminary investigation (**Hoskins and Horino, 1968**), for $\alpha_i$=0°); $\delta_i$ – max difference of the surface profile and the best-fit straight line along diameter $i$; $\alpha_i$ – slope of the best-fit straight line along the diameter $i$; $\alpha_i$' – slope of the best-fit straight line along the diameter $i$' opposite (at the opposite end) to the diameter $i$; $D$ – average specimen diameter (measured at mid-height); $\Delta l$ – 'nonparallelism' from earlier investigations (**Hoskins and Horino, 1968**).

**Figure 1.** Designations in further use and specimen with shape tolerances according to **ASTM D4543-19 (2019)** (right: modification from **Štambuk Cvitanović et al., 2015b**), further subjected to compressive strength and deformability tests (**ASTM D7012-23, 2023; ISRM, 2007**)

technical laboratory, it was observed that for limestones and rocks of a similar medium strength category (*UCS* approximately in the range of 100-150 MPa), the realistic criteria/tolerances that affect the results of mechanical properties lie somewhere between two extremes: the first is weak/soft rocks (where these influences are not pronounced, as shown by **Pells and Ferry, 1983**) and second, the strictest, required in the case of the hardest rocks such as granite. Application documents generally adopt the latter (worst case scenario) but state that, in some cases, professional judgement is required, especially if the number of samples is limited (**ASTM D4543-19, 2019; EN 1997-1, 2004; EN 1997-2, 2007**). Therefore, for the relatively common case of rocks of medium strength (limestone, dolomite, sandstone, marble), additional research on the influence of tolerances in strength and deformability tests is needed to establish behaviour models and facilitate engineering judgement. In other words, to control and optimise a process of great importance for geotechnical practice.

We propose the following hypothesis: for rocks with middle values of mechanical properties, the requirements for sample preparation should be somewhere between the extremes applicable for weak/soft rocks and the highest strength rocks. To verify our hypothesis, the effects of (non-) flatness, perpendicularity, and parallelism on *UCS*/*E*/*v* were analysed by preparing test specimens with deliberately induced shape irregularities. The specimens were then tested for strength and deformability as defined through the stress-strain curve.

In addition to directly measured influences of shape tolerances on *UCS*/*E*/*v* through a stress-strain curve (see **Figure 1**), the energy dissipation approach is also used in this study to assess the problem from the perspective of energy. Rock deformation, crack propagation, progressive damage and failure are processes characterised and driven by energy.

Therefore, in addition to the 'classical' determination of (apparent) strength and moduli, changes during the testing that occur because of increased shape irregularities were also observed through energy indicators (total, elastic and dissipated energy) in the three characteristic points marked in **Figure 1**: 1-CP closure point, 2-YP yield point and 3-*UCS* peak point/strength. In this way, the total, elastic, and dissipated energies were used to measure 'disturbance' in the compression testing of rock caused by specimen shape tolerances.

The test specimens' shape tolerances according to ASTM D4543-19 are depicted in **Figure 1**, and the origins of the tolerances are shown in **Figures 2** and **3**.

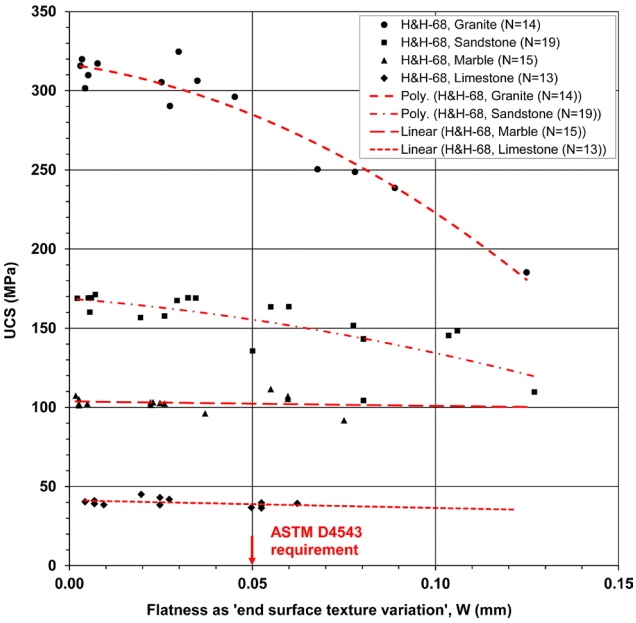


**Figure 2.** Influence of non-flatness on *UCS*, expressed as $W \approx 2\delta$ (max. profile height or peak-to-peak amplitude of surface profile at one end of the specimen) from the preliminary investigations (**Hoskins and Horino, 1968**; shown as H&H-68 in the figure), recalculated to SI units (added trendlines and ASTM requested tolerance)

As shown in **Figure 2**, the influence of flatness on *UCS* becomes greater with the increased (category of) *UCS*. For granite and rocks of the highest strength, a significant decrease in strength with *W* is noticeable, reflecting the value of the 'worst case' set tolerance according to ASTM D4543. For rock with a strength of about 100 MPa (in this case, marble and limestones of higher strength than those shown), there was no significant decrease in strength in the range covered by the test results, up to about 0.08 mm. The *UCS* may start to decrease at some value of flatness *W* outside the range shown, but there are not enough data. It can be assumed that this kind of moderate behaviour between extremes also applies to limestones and other rock types of similar strength, which is of interest in this research.

Furthermore, it is possible to determine at which *W* value *UCS* will start to decrease relative to some reference value if statistical variabilities and risks are considered. For sandstones and rocks with *UCS* around 150 MPa, the trend of decreasing strength is somewhat more pronounced, but not as it is for granite. In fact, for all rocks in the medium strength category of 100–150 MPa, some 'average' value of the required flatness tolerance can be expected. The same can be determined by researching the behaviour model for the influence of flatness *W*.

As shown in **Figure 3**, although *UCS* decrease was determined in the 'flat head' test, with the perpendicularity tolerance in the ASTM D4543 standard set at a 'safe value', no decrease in strength was determined for any type of rock in the case of the spherical head test (compression machines with spherical head/seat) until the slope of the specimen end of approximately $\alpha_i = 0.9°$. As with the previous impact of *W*, it is necessary to expand the range of research and establish behaviour models for the impact of angular specimen irregularities in the case of modern test equipment with a spherical seat.

Considering the findings above, some optimisation is required. This study shows the results of an experimental research programme conducted on 90 limestone specimens. The results determined behaviour models for the influence of shape tolerances on mechanical properties and suitable values of 'medium' tolerances for limestone and similar rocks with strength in the range of 100–150 MPa. Behaviour models obtained directly from experimental results constitute the so-called 'natural models'. Statistical models were also determined by further statistical analysis and multiple regression. In addition, the influence of tolerances on energy dissipation characteristics was analysed, whereby the energy approach enriches and confirms the conclusions from natural and statistical models. By applying the obtained results, optimisation and savings are possible in further procedures as part of the geotechnical design.

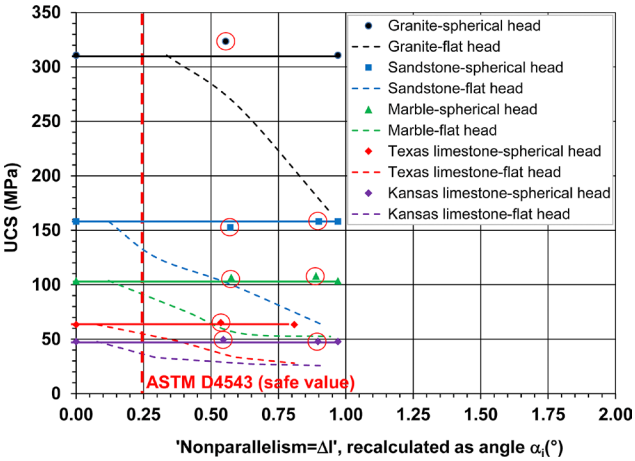


**Figure 3.** Influence of 'nonparallelism' $\Delta l$ from the preliminary investigations (**Hoskins and Horino, 1968**) on *UCS*, recalculated to SI units (*UCS*) and expressed as an angular deviation $\alpha_i$ in **Figure 1** (added current ASTM tolerance)

## 2. Research methodology

The previously unpublished part of earlier research is presented in the following sections, where the results (verified statistically and numerically) are newly re-interpreted based on energy dissipation. The methodology (since described with other results; **Štambuk Cvitanović et al., 2015b**) is given to the extent necessary from a scientific point of view.

### *2.1. Preparation of specimens with targeted shape irregularities (tolerances)*

For the planned research, 90 cylindrical specimens with initial dimensions $D \approx 54$ mm (diameter) and

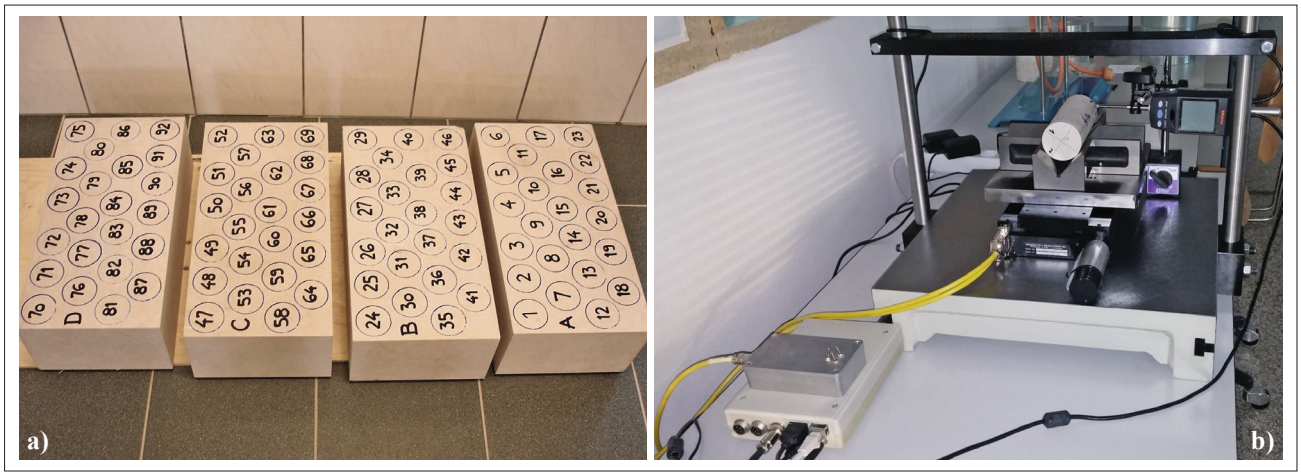


**Figure 4.** Preparation and further 'recording' of test specimens: a) block samples; b) newly developed equipment: Coordinate Measuring System (CMS), a device for automatic recording and verification of rock cylindrical specimens

$L/D \approx 2.5$ (diameter to length ratio) were drilled from four block samples. The samples were obtained in the same quarry and main stone block of limestone of the Upper Cretaceous - Senonian ($K_2^3$) without visible cracks, veins, and discontinuities (see **Figure 4a**).

Given the research objectives of better characterisation, optimisation, and establishment of the behaviour models for limestones and similar rocks, to obtain reliable input data (with a minimal influence of human factor), Coordinate Measuring System (CMS) (**Štambuk Cvitanović and Đukić, 2014**) was developed for quick and accurate recordings of surface profiles along arbitrary lines on the surface of a cylindrical test specimen (see **Figure 4b**). Discrete manual readings are replaced with automatically recorded continuous curves with the density of readings at will along the diameters and side straight lines. The curves of surface profiles are determined so that the readings of one or more displacement gauges in contact with the specimen and the positions of these readings (using an optical sensor) are simultaneously recorded within the automatic acquisition system. Thus, it is possible to draw individual surface profiles and sections through the specimen with high resolution and accuracy and 5–6 times faster than the manual process.

Initially, 90 roughly prepared specimens (without grinding, only saw cut, both in field and laboratory conditions) were analysed using CMS (i.e. resulting surface profiles). On roughly prepared samples without grinding, the flatness of the ends $W$ ranges from about 0.04–0.5 mm, perpendicularity and parallelism up to about 2°, and side straightness about 0.3-0.8 mm (the larger part of the specimens meets the ASTM requirement $\Delta_{max} <$ 0.50 mm). This also provided guidelines for the shape tolerance ranges in the research, as larger irregularities in the shape of the specimens would not even appear in the laboratory.

Anisotropy effects are avoided by always drilling blocks in the same direction; to verify rock homogeneity, non-destructive tests were performed on all specimens. The density $\rho$ (average value 2550 kgm$^{-3}$), the velocity of longitudinal (primary) elastic waves by ultrasonic technique $v_P$ (average 4953 m/s) and Schmidt Rebound Hardness $HR$ (representative Schmidt hammer rebound number 37.5 according to **ISRM, 1978**) were determined (**Štambuk Cvitanović, 2012**). The coefficients of variation $Cv$ for $\rho$ and $v_P$ are small values (0.6% and 1.6%, respectively), and the biggest changes of the same properties are also adequately small (2% and 8%, respectively). In previous investigations (**Hoskins and Horino, 1968**), the maximum wave velocity change was 7%. The coefficient of variation for $HR$ values is also small, at only 2%. From all obtained $Cv$ values, we concluded that the variability of index properties is low; consequently, the degree of homogeneity of the specimens is high.

The following properties of limestone rock were also determined based on the remains of the material: content of $CaCO_3$ = 96–100% (according to the proportion of MgO and CaO, the rock is dolomitic limestone), specific gravity $G_s$ = 2.71, moisture content $w$ = 0.04% (specimens stabilised to laboratory conditions), and porosity $n$ = 4.84–6.68%.

In general, it is possible to use different variables for the end flatness "$R$", parallelism "$P$" and perpendicularity "$O$" (abbreviated designations). In this study, some values proved to be the most relevant. Since the difference between the surface profile and trend line $\delta_i$ (see **Figure 1**) as a measure of flatness is not suitable for concave and convex profiles, and to better correlate the results with previous research, the end flatness is further expressed using $R = W$ (mm) as the maximum surface profile height (peak-to-peak amplitude).

Instead of parallelism determined from specimen 2D section (see **Figure 1**) $\Delta\alpha_i = \alpha_i - \alpha_i'$, the parallelism measure $P = \Delta\varphi$ (°) is used as the calculated (spatial, 3D) angle between planes of upper and lower specimen end; perpendicularity (3D) $O = \varphi''$ (°) is calculated as the slope of lower specimen end. Such definitions also have

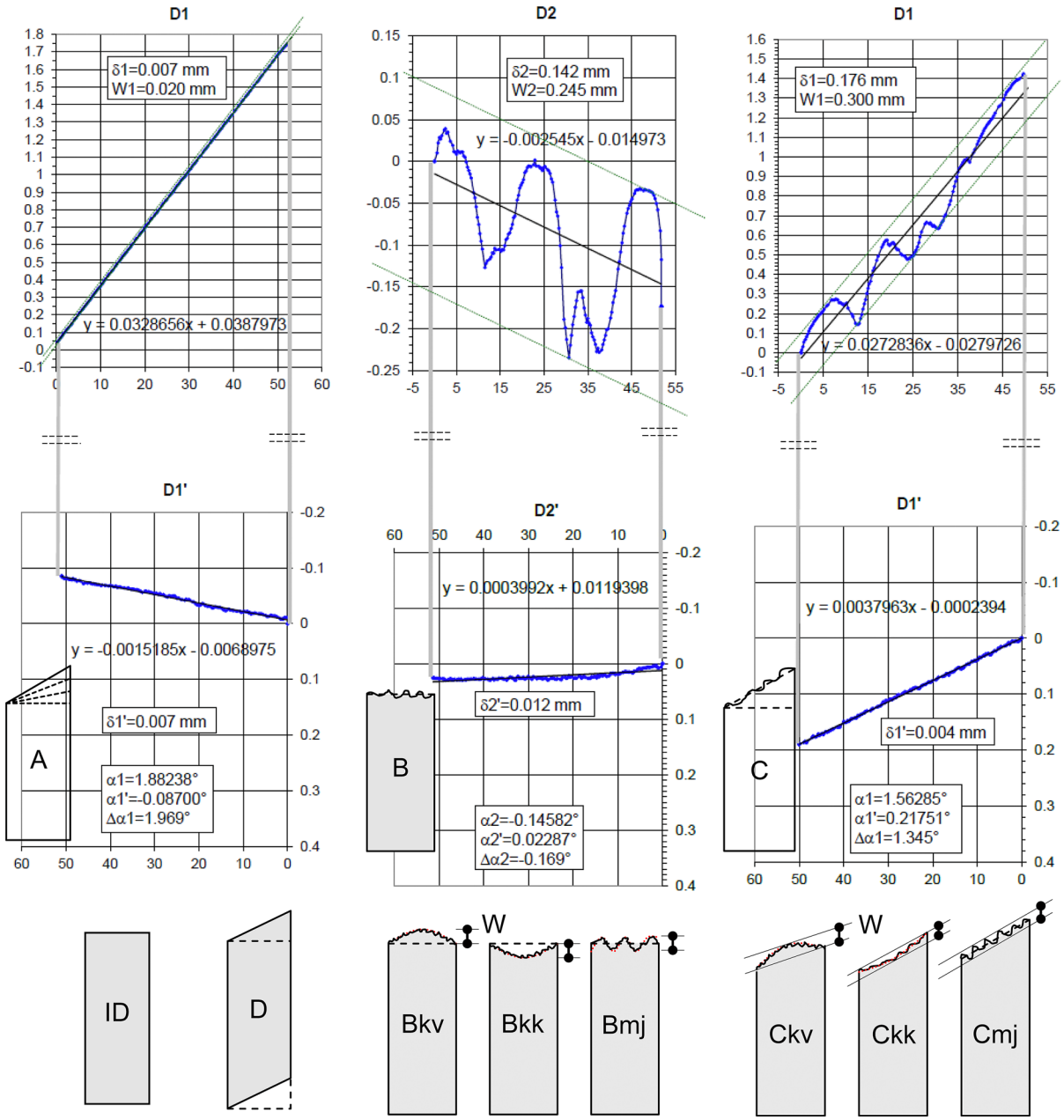


**Figure 5.** Above: typical sections through the specimens obtained with the CMS device - examples of specimens with a deviation of parallelism (group A), flatness (B) and combined parallelism and flatness (C); bottom: other groups (ID, D) and subgroups of specimens (convex, concave and mixed profile types)

a deeper physical meaning because after placing the specimen on the lower pressure plate of the compression machine and the consequent initial inclination of the axis of the specimen for $\varphi''$, the upper pressure plate with spherical seating will adjust to the specimen and incline for $\Delta\varphi$ in relation to the lower specimen end and the lower pressure plate. That is, the perpendicularity on the upper specimen end is the sum of the perpendicularity on the lower specimen end and parallelism.

Adequate (2D) variables according to ASTM from **Figure 1** were kept as informative and control values (for example, for all specimens, the difference $|\Delta\varphi - \Delta\alpha_i|$ did not exceed 0.07°). The cosine error (difference between the measurement of $W$ and $\delta$ in the local (CMS) and the global coordinate system, where the y-axis of the global coordinate system is the vertical axis of the compression testing machine) is negligible because all angular deviations are up to 2°.

Considering the above-mentioned definitions of $R$, $P$ and $O$, specimens with intentionally produced shape irregularities were prepared so that they belong to the planned groups and subgroups (see **Figure 5**):

- ID: 'ideal' specimens without (with minimal) shape deviations that do not affect the mechanical properties (tolerances according to ASTM D4543, where the known measurement uncertainties were also

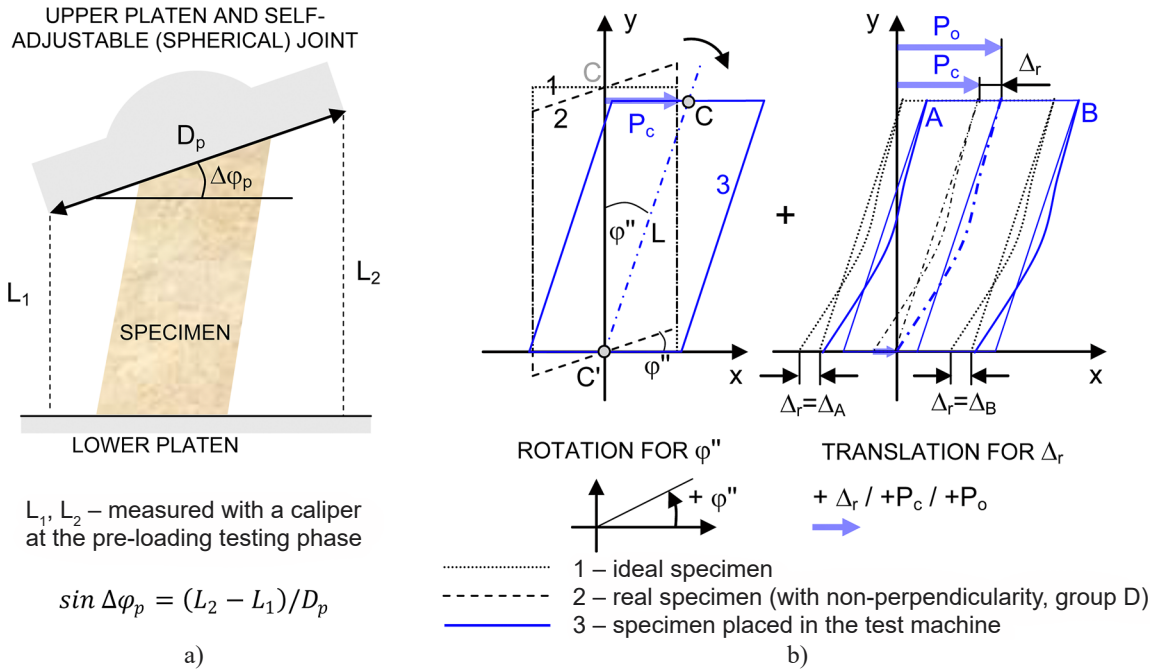


**Figure 6.** Specimen parameters (in addition to basic *R*/*P*/*O*): a) measuring of parallelism during testing as the angle between pressure platens; b) additional parameters to describe deviations of coaxial alignment or concentricity

considered); in addition to 11 basic ID specimens (ID-o), 8 additional ones (ID-d) were also observed, which are specimens from groups A and B that still meet the ID criteria.

- A: intentionally made only with a non-parallelism of $P = \Delta\varphi$ = 0.2–2°, while other tolerances were within small favourable values (24 specimens).
- B: only non-flatness of the upper end of $R = W$ = 0.03–0.5 mm; to assess the impact of the type of 'waviness' further classified into convex (Bkv), concave (Bkk) and mixed (Bmj) subgroups (24 specimens, of which 9 Bkv, 8 Bkk and 7 Bmj).
- C: combined non-parallelism of $P = \Delta\varphi$ = 0.5–2.3° and non-flatness of $R = W$ = 0.04–0.3 mm; further classified according to the type of waviness as convex (Ckv), concave (Ckk) and mixed (Cmj) subgroups (23 specimens, of which 7 Ckv, 8 Ckk and 8 Cmj).
- D: only non-perpendicularity of the lower end to the axis of the specimen within the range of $O = \varphi''$ = 0.2–2.2°, where the upper end remains parallel to the lower one (8 specimens).

Preparing the specimens required a combination of machine processing (drilling, cutting, circumferential surface grinding in the lathe if necessary, grinding of the ends) and manual processing of the upper base of the sample until specimens with target *R*/*P*/*O* values according to the mentioned groups/subgroups were obtained. During grinding, the direction of the largest slope on the upper specimen end was marked and known using an additional slope adjustment assembly with a V-block as a specimen holder on the surface grinder. In these procedures, the treatment of almost any specimen was repeated several, sometimes 5–10 times. Therefore, the CMS device for checking and verifying of specimens was invaluable, allowing a quick and quality view of actual surfaces. By repeating the preparing and recording cycles, all specimens were finally shaped within a predefined range of flatness, parallelism and perpendicularity, in which the range of certain shape irregularities within the group is evenly covered.

Verification of the achieved shape tolerances involved the following procedures:

- At least two determinations of the input *R*/*P*/*O* parameters of each specimen using the CMS: after specimen preparation and immediately before placement in the compression machine.
- Calculation of angular irregularities *P* and *O* in two ways: in the (2D) manner described in **Figure 1** and from the slopes of directions (two and two orthogonal diameters), which spatially define planes of the upper and lower ends, as well the spatial angle between them (primary, 3D).
- Additional control of the angle $P = \Delta\varphi$ during the compressive test pre-load phase by measuring the angle $\Delta\varphi_p$ between the pressure plates (see **Figure 6a**).
- Double determination of side straightness, where side surfaces were first recorded as shown in **Figure 1** for three straight lines spaced at 120°. However, for final recording just before the uniaxial test, two diametrically opposed lines were taken to introduce some new properties (see **Figure 6b**).

Finally, additional parameters are defined, which describe the (straightness) deviation of the specimen axis from coaxiality/concentricity and depend on the meas-

**Table 1.** Final input parameters - achieved (induced) shape tolerances of the specimens before uniaxial tests

| Group and number of specimens | Flatness, $R = W$ (mm) | Parallelism, $P = \Delta\varphi$ (°) | Perpendicularity – main, $O = \varphi''$ (°) | Perpendicularity – additional, $O = P_c$ (mm) | Perpendicularity – additional, $O = P_o$ (mm) |
|---|---|---|---|---|---|
| **ID-o** N = 11 (i) | 0.018 | 0.146 | 0.210 | 0.453 | 0.569 |
| **ID** = (ID-o) + (ID-d) N = 11 + 8 (ii) | 0.022 | 0.184 | 0.199 | 0.439 | 0.562 |
| **A** N = 24 | 0.021 | **0.228 - 1.958** | 0.189 | 0.432 | 0.493 |
| **B** N = 24 (iii) | **0.030 - 0.522** | 0.209 | 0.173 | 0.400 | 0.573 |
| **C** N = 23 (iv) | **0.044 - 0.333** | **0.536 - 2.266** | 0.250 | 0.574 | 0.718 |
| **D** N = 8 | 0.029 | 0.158 | **0.231 - 2.151** | **0.535 - 4.092** | **0.814 - 4.169** |

If $R/P/O$ are small (standard, strict) values, the average value for a particular group is given, and if $R/P/O$ are intentionally caused as the large deviations for research purposes, the range within which the values are approximately evenly distributed for the specified number of specimens in the group is indicated.
(i) 11 basic (ID-o) 'ideal' specimens
(ii) 11 ID-o and 8 additional (ID-d) ideal specimens (4 specimens each from groups A and B that still meet the criteria for ID)
(iii) Out of 24 specimens, 9 have a convex (Bkv), 8 are concave (Bkk), and 7 have a mixed (Bmj) profile type on the upper end.
(iv) Out of 23 specimens, 7 have a convex (Ckv), 8 are concave (Ckk), and 8 have a mixed (Cmj) profile type on the upper end.

ured side straightness and perpendicularity on the lower specimen end. In **Figure 6b**, the change (relative to the ideal specimen shape) caused by rotation for $\varphi''$ on the lower end is reflected by the displacement of the specimen centre $P_c$ on the upper specimen end:

$$P_c = L \cdot \sin\sin\varphi'' \quad (1)$$

where:

$P_c$ - horizontal displacement of the specimen centre/axis at the upper end, the initial, caused by non-perpendicularity of the lower end $\varphi''$, measured from the y-axis of the global coordinate system (vertical machine axis that passes through the centre of the lower pressure platen),

$L$ - specimen length,

$\varphi''$ - slope of the lower end (perpendicularity).

If diametric changes (side straightness deviations) are now added to the specimen position, the axis of the specimen will have new displacements across the length and curvature - change in shape. Therefore, the centre of the lower end will not coincide with the centre of the lower platen. To centre the specimen, it must be translated equally to the displacement of the side straight line (at the lower end level, in the reference section). The total displacement of the specimen axis will be:

$$P_o = P_c + \Delta_r \quad (2)$$

$P_o$ - total horizontal displacement of the upper-end centre/axis because of the lower-end non-perpendicularity and side straightness deviations (measured in the global coordinate system),

$\Delta_r$ - edge side straightness deviation (displacement/shift of the side straight line at the level of lower end); this can be determined from the surface profile recorded along the opposing side straight lines A and/or B.

Value $P_o$ reflects both the influences of angular deviations at the specimen ends and side straightness deviations, which should be considered because the first affects the non-uniformity of deformations, and the second affects the non-uniformity of stress distribution and misalignment of centres of the ends of the specimen with the test machine's vertical axis (**Podnieks et al., 1972**). These impacts can be observed as a change of shape in the coaxial alignment or concentricity deviations. They lead to the apparent properties of the stress-strain curve in its initial part and, in general, to the impacts on deformability (especially on the apparent Poisson's ratio, which includes both axial and radial deformations and is the most 'sensitive' parameter, as investigated by **Dong et al., 2021**). The influence of edges on the $\sigma$-$\varepsilon$ curve is described (**Hudson and Harrison, 2000**) as an equal cause of the initial curve shape, together with the known closure of microcracks. In general, the authors did not address the deviations of the side surface and the axis of the specimen.

From the above, together with the flatness and parallelism, perpendicularity as the third input parameter can be expressed by one of the values $\varphi''$, $P_c$ or $P_o$, wherein $P_c$ in data 'pulls' the specimen length and $P_o$ also the side surface. $P_o$ (and $P_c$) can be expressed relative to the diameter $D$.

In the described manner, the final input parameters $R/P/O$ were determined and accepted (see **Table 1**). $P_o$

was analysed in detail and determined afterwards for specimens with measured Poisson's ratio (46 of 90 specimens) because of its significance in further testing (influences on $v$, results in Section 3).

**Table 1** shows that the ranges of realised shape deviations are relatively large compared to ASTM values and previous research shown in **Figures 2** and **3**, with non-flatness generally ranging up to 0.5 mm, and angle deviations up to 2°.

### 2.2. Testing – equipment and procedures

Using described specimens with the induced shape deviations, further investigations included determining strength and elastic moduli of intact rock core specimens according to the widely recognised ASTM D7012 standard (**ASTM D7012-23, 2023**). Test equipment consists of a servo-controlled spherically seated rock testing system (capacity 2000 kN, stiffness 4.9 MN/mm between upper and lower plate). At the time of research, this was located in an accredited geotechnical laboratory (Institute IGH, Split, Croatia). Two configurations enable measurements of deformations and strains during uniaxial tests: a) only LVDTs - Linear Variable Differential Transformers (50 specimens) and b) LVDTs and strain gauges at the same time, i.e. connected to the same control and acquisition system (40 specimens).

The first configuration includes three LVDTs set to measure axial deformations and three LVDTs with an angular spacing of 120° set to measure radial deformations, which enables the measurement of Poisson's ratio. In doing so, two LVDTs measure the axial deformation at the middle third of the specimen height (using two rings attached to the specimen and measuring base length $L_b$ = 50 mm in **Figure 1**) at positions (along the side straight lines) corresponding to the lowest "A" and the highest "B" edge of the specimen (defined by the known diameter or direction of the largest slope on the upper end). Additional LVDT measures the deformation along the entire length of the specimen at the 'neutral' position "C" (perpendicular to the direction of the largest slope). The latter is included because such a measurement is relatively common in practice, and the results reflect the effects of shape irregularities at the ends of the specimen to a greater extent. In this way, both Young's moduli are obtained simultaneously: the modulus measured at the centre (middle third) of the specimen length and the modulus measured on the entire specimen length.

The second configuration is the same in terms of measuring axial deformations (LVDTs at positions A, B and C), but along the side straight lines at positions A and B strain gauges connected to the same measuring system are additionally placed on the specimen surface to directly measure axial strains in the mid-height of the specimen. For the rock type (largest grain) and the coefficient of thermal expansion, we chose strain gauges with a measuring base length of 10 mm and 350 Ω resistance (manufacturer HBM). In this configuration, it is impossible to measure radial deformations due to system limitations.

**Štambuk Cvitanović et al. (2015b)** describe the testing equipment and the procedure in detail, including evaluating the effects of friction and stress/strain non-uniformity at the specimen ends. Since the influences originating only from shape tolerances $R/P/O$ are the main research goal, for all specimens the mechanical properties $UCS/E/v$ were tested according to the ASTM procedure (at the time of research **ASTM D7012-10, 2010**) with strict compliance to the requirements of the standard and with all the same conditions, except that the shape tolerances were variable. Before the uniaxial test, each sample was examined visually, dimensions and density were measured again, and the final surface profiles were recorded using CMS. The tests were performed with a controlled displacement rate of 0.001 mm/s (failure within 10–15 min). During testing, all important phenomena, including characteristic failure modes, were carefully documented (see **Figure 7**).

### 2.3. Calculation of mechanical and energy dissipation properties

The research programme included testing of all specimens in uniaxial compression when there is no obligation to obtain a complete stress-strain curve in the post-failure region (although for 1/3 of the specimens the post-failure region is very well covered). The following values were continuously recorded: time, force, displacement of LVDT which controls experiment, axial A/B/C deformations, radial A/B/C deformations and axial A/B strains measured with strain gauges. After processing all the data and plotting $\sigma$-$\varepsilon$ curves, the mechanical and energy dissipation properties were calculated as follows:

Mechanical properties

1. $UCS$ = uniaxial compressive strength (MPa)

$$UCS = \frac{max.\,force}{cross-sectional\ area} = \frac{F_{\max}}{A} = \frac{F_{\max}}{\left(\frac{D^2\pi}{4}\right)} \quad (3)$$

2. $UCS_{50}$ = equivalent UCS for specimen with 50 mm diameter (**Hoek and Brown, 1980**)

$$UCS_{50} = \frac{UCS}{\left(\frac{50}{D}\right)^{0.18}} \quad (4)$$

3. $E$ = Young's modulus – primary (GPa); calculated as the "average" modulus of approximately linear portion of $\sigma$-$\varepsilon$ curve for stress level of 50% $UCS$, from stress increment $\Delta\sigma$ = (40%–60%) $UCS$ and the corresponding increment of axial deformation $\Delta\varepsilon$, wherein the deformations are measured in the mid-height of the specimen using the LVDTs


**Figure 7.** Characteristic failure modes with indicated specimen groups and subgroups

$$E = \frac{\Delta\sigma}{\Delta\varepsilon} \tag{5}$$

*4.* $E_{sg}$ = Young's modulus – additional; calculated from the increment $\Delta\varepsilon_{sg}$ of axial strains $\varepsilon_{sg}$ measured directly on the specimen using strain gauges, again for $\Delta\sigma$ = (40%–60%) *UCS*

$$E_{sg} = \frac{\Delta\sigma}{\Delta\varepsilon_{sg}} \tag{6}$$

*5.* $E_L$ = Young's modulus – approximate; calculated from the increment $\Delta\varepsilon_L$ of axial deformations $\varepsilon_L$ measured on the entire specimen length, also for $\Delta\sigma$ = (40%–60%) *UCS*

$$E_L = \frac{\Delta\sigma}{\Delta\varepsilon_L} \tag{7}$$

*6.* $E_{L,2}$ = equivalent $E_L$ for the specimen length to diameter ratio of $L/D$ = 2.0 (**Thuro et al., 2001**)

$$E_{L,2} = E_L \cdot \left(1.24 - 0.33 \cdot \ln\left(L/D\right)\right) \tag{8}$$

This applies only when deformation is measured between the pressure platens. A similar relationship for the *UCS* has no practical significance, since, for $D$ = 50–54 mm, the change in *UCS* is less than 2% (**Hoek and Brown, 1980; Thuro et al., 2001**).

**Table 2.** Summary of the mechanical properties and main test results

| Group | Property | *UCS* (MPa) | $UCS_{50}$ (MPa) | *E* (GPa) | $E_{sg}$ (GPa) | $E_L$ (GPa) | $E_{L,2}$ (GPa) | *v* | $v_T$ | $v_L$ |
|---|---|---|---|---|---|---|---|---|---|---|
| **ID-o** | *Min* | 119.033 | 120.757 | 45.822 | 59.068 | 41.051 | 41.590 | 0.244 | 0.257 | 0.230 |
| | *Max* | 136.068 | 136.775 | 58.848 | 60.103 | 52.641 | 49.301 | 0.313 | 0.320 | 0.291 |
| | $\bar{X}$ | 128.386 | 129.450 | 51.066 | - | 47.036 | 45.080 | 0.284 | 0.295 | 0.260 |
| | *s* | 6.244 | 5.648 | 4.159 | - | 3.654 | 2.183 | 0.022 | 0.021 | 0.024 |
| | *Cv* | 0.049 | 0.044 | 0.081 | - | 0.078 | 0.048 | 0.077 | 0.072 | 0.094 |
| **ID** (ID-o and ID-d) | *Min* | 119.033 | 120.757 | 45.822 | 50.300 | 41.051 | 40.679 | 0.244 | 0.257 | 0.230 |
| | *Max* | 136.077 | 138.136 | 60.405 | 60.103 | 52.641 | 49.301 | 0.313 | 0.320 | 0.305 |
| | $\bar{X}$ | 128.582 | 129.778 | 51.522 | 56.480 | 46.982 | 44.710 | 0.280 | 0.290 | 0.264 |
| | *s* | 5.607 | 5.464 | 4.324 | 3.857 | 3.358 | 2.342 | 0.022 | 0.022 | 0.024 |
| | *Cv* | 0.044 | 0.042 | 0.084 | 0.068 | 0.071 | 0.052 | 0.080 | 0.078 | 0.091 |
| **A** | *Min* | 113.531 | 115.252 | 40.915 | 48.180 | 43.131 | 42.276 | 0.246 | 0.263 | 0.244 |
| | *Max* | 136.077 | 138.136 | 62.278 | 59.980 | 50.388 | 47.840 | 0.374 | 0.362 | 0.305 |
| | $\bar{X}$ | **127.079** | **129.003** | **52.428** | **55.531** | **46.650** | **44.231** | 0.302 | **0.302** | 0.284 |
| | *s* | **5.010** | **5.089** | 6.057 | **3.376** | **1.773** | **1.534** | 0.051 | 0.041 | **0.025** |
| | *Cv* | **0.039** | **0.039** | 0.116 | **0.061** | **0.038** | **0.035** | 0.169 | 0.136 | **0.089** |
| **B** | *Min* | 48.575 | 48.719 | 40.558 | 50.0 | 33.541 | 30.569 | 0.190 | 0.198 | 0.131 |
| | *Max* | 129.196 | 129.625 | 60.405 | 63.299 | 50.141 | 46.317 | 0.308 | 0.319 | 0.281 |
| | $\bar{X}$ | 95.728 | 96.288 | **52.518** | **56.474** | 40.020 | 37.169 | 0.247 | 0.258 | 0.212 |
| | *s* | 23.026 | 23.200 | 5.240 | **2.892** | 5.094 | 4.741 | 0.042 | 0.041 | 0.060 |
| | *Cv* | 0.241 | 0.241 | 0.100 | **0.051** | 0.127 | 0.128 | 0.170 | 0.158 | 0.284 |
| **C** | *Min* | 62.636 | 62.728 | 45.098 | 51.214 | 33.384 | 30.610 | 0.202 | 0.221 | 0.165 |
| | *Max* | 127.013 | 127.232 | 57.118 | 62.206 | 45.793 | 42.922 | 0.300 | 0.296 | 0.261 |
| | $\bar{X}$ | 108.358 | 108.962 | **51.820** | **56.032** | 42.478 | 39.530 | 0.256 | 0.259 | 0.213 |
| | *s* | 16.939 | 17.143 | **3.528** | **3.934** | **3.056** | 2.933 | 0.026 | **0.023** | 0.028 |
| | *Cv* | 0.156 | 0.157 | 0.068 | 0.070 | 0.072 | 0.074 | 0.100 | 0.089 | 0.131 |
| **D** | *Min* | 114.422 | 116.119 | 40.365 | - | 39.952 | 40.345 | 0.220 | 0.215 | 0.190 |
| | *Max* | 134.917 | 136.962 | 48.032 | - | 48.373 | 45.878 | 0.325 | 0.341 | 0.327 |
| | $\bar{X}$ | **122.906** | **124.638** | 45.098 | - | **45.252** | **42.984** | **0.289** | **0.293** | 0.293 |
| | *s* | **6.215** | **6.408** | **2.577** | - | **2.515** | **1.773** | 0.040 | 0.048 | 0.052 |
| | *Cv* | **0.051** | **0.051** | **0.057** | - | **0.056** | **0.041** | 0.137 | 0.163 | 0.178 |

*Min* – minimum value, *Max* – maximum value, $\bar{X}$ – mean value, *s* – standard deviation, $Cv = s/\bar{X}$ – coefficient of variation
Bold – parameters better or close (differences < 5%) to the reference values from the ID group and published data on "precision and bias" as the product of the interlaboratory testing programme (**ASTM D7012-23, 2023**)

*7.* $\nu$ = Poisson's ratio – primary; calculated from the slopes of radial and axial $\sigma$-$\varepsilon$ curves, from the increments of radial deformations $\Delta\varepsilon_r$ and axial deformations $\Delta\varepsilon$, with the same $\Delta\sigma$ as in the calculation of *E*

$$\nu = -\frac{slope\ of\ axial\ curve}{slope\ of\ radial\ curve} = -\frac{\frac{\Delta\sigma}{\Delta\varepsilon}}{\frac{\Delta\sigma}{\Delta\varepsilon_r}} = \frac{\Delta\varepsilon_r}{\Delta\varepsilon} \quad (9)$$

*8.* $\nu_T$ = Poisson's ratio – equivalent to Poisson's ratio $\nu$ in **Equation 9**, but from trend lines; calculated from the slopes of the best-fit straight lines of radial and axial $\sigma$-$\varepsilon$ curves (from all included points or measurements, not just two end points), with the same $\Delta\sigma$ as in the calculation of *E*

$$\nu_T = -\frac{slope\ of\ axial\ curve}{slope\ of\ radial\ curve} = \frac{\Delta\varepsilon_{r,T}}{\Delta\varepsilon_T} \quad (10)$$

*9.* $\nu_L$ = Poisson's ratio – additional, corresponding to $E_L$ modulus; calculated from increments of axial $\Delta\varepsilon_L$ and radial $\Delta\varepsilon_r$ deformations, where the axial deformations $\varepsilon_L$ are measured on the entire specimen length, and for the same $\Delta\sigma$ as for $E_L$

$$\nu_L = -\frac{slope\ of\ axial\ curve}{slope\ of\ radial\ curve} = \frac{\Delta\varepsilon_r}{\Delta\varepsilon_L} \quad (11)$$

### *Energy dissipation properties*

*10.* $W_t$ = total energy (kJ/m³), which represents the total area under the $\sigma$-$\varepsilon$ curve, i.e. the sum of elastic energy $W_e$ and dissipated energy $W_d$

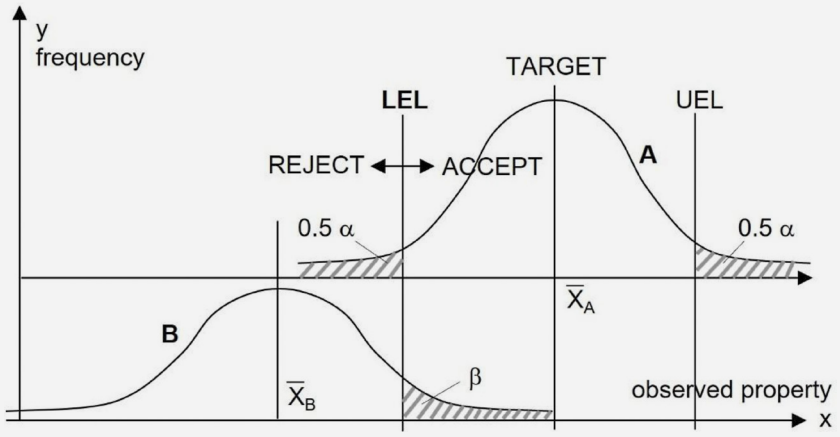


A = acceptable result (without effects of the specimen shape tolerances)
B = unacceptable result (affected by influences of the specimen shape tolerances)
$P_A$ = probability of acceptable result appearance - area under normal curve A
$\alpha$ = probability / risk of rejecting acceptable result ('producer's risk')
$P_B$ = probability of unacceptable result appearance – area under normal curve B
$\beta$ = probability / risk of accepting unacceptable result ('consumer's risk')
Reducing $\alpha$ increases $\beta$. $\alpha$ and $\beta$ are probabilities of the errors of the 1st and 2nd kind.
*UEL* is of importance only for the Poisson's ratio.

**Figure 8.** Determination of engineering limits (**U.S. Department of Transportation, 1977**)

$$W_t = \int_0^{\varepsilon} \sigma d\varepsilon = \sum_{i=1}^{n} \frac{1}{2}\left(\sigma_{i+1} + \sigma_i\right)\left(\varepsilon_{i+1} - \varepsilon_i\right) = \\ = W_e + W_d \quad (12)$$

*11.* $W_e$ = elastic energy (kJ/m$^3$)

$$W_e = \frac{1}{2}\sigma\varepsilon_e = \frac{\sigma^2}{2E} \quad (13)$$

where $\varepsilon_e$ is the elastic portion of axial strain. **Equation 13** is valid assuming that the modulus of elasticity in unloading is equal to Young's modulus $E$, according to **Equation 5**.

*12.* $W_d$ = dissipated energy (kJ/m$^3$)

$$W_d = W_t - W_e \quad (14)$$

*13.* $\lambda$ = energy dissipation coefficient (or energy dissipation ratio), as the ratio of $W_d$ and $W_e$

$$\lambda = \frac{W_d}{W_e} \quad (15)$$

**Equations 12** to **15** refer to a specific point of the $\sigma$-$\varepsilon$ curve (e.g. points 1-CP, 2-YP and 3-*UCS* in **Figure 1**).

## 3. Results

The summarised and consolidated results of the research are presented below. Verification of the results using statistical and numerical methods, as well as their re-interpretation using an energy approach, are also described.

### *3.1. Natural models*

As the Introduction explains, 'natural models' imply behaviour models obtained directly from experimental results, where shape tolerances *R*/*P*/*O* correlate with mechanical properties *UCS*/*E*/*v*. **Table 2** shows the primary results of the uniaxial compression tests for all mechanical properties and all specimen groups.

#### 3.1.1. Specimens from the control group – determination of engineering limits

The testing programme included 19 'ideal' specimens with small/minimal *R*/*P*/*O* values (see **Table 1**, group ID). Compressive tests and calculations are described in Sections 2.2 and 2.3, and characteristic $\sigma$-$\varepsilon$ diagrams are given in Section 3.3 together with energy curves. Double shear and shearing along a single plane across the entire specimen appear as typical failure modes under uniaxial compression (see **Figure 7**), accompanied by explosive failures and smooth $\sigma$-$\varepsilon$ curves with no signs of local failure. Based on the obtained coefficients of variation (see **Table 2**), the natural variability at the level of one standard deviation for strength (*UCS* and $UCS_{50}$) is 4–5%, and for moduli and Poisson's ratios, 5–9%.

The results of the (extended) ID control group were further used to determine the inherent variability of intact rock mechanical properties (rock as a *natural* material). The limits within which this variability falls are "engineering limits": *LEL* is the Lower Engineering Limit, and *UEL* is the Upper Engineering Limit (see **Figure 8**).

**Table 3.** Final accepted (reference) engineering limits and means in this study and the reference statistical data from the interlaboratory testing programme

| **Property** | ***UCS*** **(MPa)** | $UCS_{50}$ **(MPa)** | ***E*** **(GPa)** | $E_{sg}$ **(GPa)** | $E_L$ **(GPa)** | $E_{L,2}$ **(GPa)** | $\nu, \nu_T$ | $\nu_L$ | ***ν*** **general** |
|---|---|---|---|---|---|---|---|---|---|
| Average values and engineering limits – this study (N=43) | | | | | | | | | |
| $\bar{X}$ | 127.531 | 128.845 | 51.614 | 56.281 | 46.681 | 44.331 | 0.29 | 0.27 | 0.28 |
| *LEL* | 116.4 | 117.6 | 43.4 | 50.1 | 41.5 | 40.4 | 0.25 | 0.23 | 0.24 |
| *UEL* | 138.7 | 140.1 | 59.9 | 62.5 | 51.9 | 48.3 | 0.33 | 0.31 | 0.32 |
| Statistical properties of the rock with corresponding (medium) strength category (**ASTM D7012-23, 2023**) | | | | | | | | | |
| Tennessee Marble | *UCS* (MPa) | | $E_{50\%}$ (GPa) | | | | $\nu_{40\text{-}60\%}$ | | |
| Average value $\bar{X}$ | 142.0 | | 74.2 | | | | 0.33 | | |
| Repeatability limit *r* | 20.4 | | 10.1 | | | | 0.07 | | |
| Reproducibility limit *R* | 38.0 | | 12.3 | | | | 0.09 | | |
| $s_r = r / 2^{1.5}$ | 7.212 | | 3.571 | | | | 0.025 | | |
| $s_R = R / 2^{1.5}$ | 13.435 | | 4.349 | | | | 0.032 | | |
| $Cv_r = s_r / \bar{X}$ | 0.051 | | 0.048 | | | | 0.075 | | |
| $Cv_R = s_R / \bar{X}$ | 0.095 | | 0.059 | | | | 0.096 | | |
| Number of included results $N_R$ | 35 | | 40 | | | | 120 | | |
| | 7 labs x 5 repl. | | 8 labs x 5 replications | | | | 6 labs x 5 spec. x 4 repl. | | |

*LEL* and *UEL* represent limits within which the values of *UCS*/*E*/*ν* should vary due to the natural variability of the rock material, which exists even under ideal conditions without the influence of shape tolerances. A comprehensive assessment of *UCS*/*E*/*ν* dispersion (**Štambuk Cvitanović, 2012**) included measurement uncertainty ($U = 2s$) as a generally accepted measure of dispersion, dispersion for concrete (5% fractile) and data from a wider study published in **ATM D7012-23 (2023)** (see **Table 3**). This interlaboratory testing programme provides data on the mean values and limits of repeatability *r* and reproducibility *R* for the mechanical properties of several types of rocks. The meaning of *r* (*R*) is that the probability is about 95% that two test results obtained in the same laboratory (different laboratories) on the same material will not differ by more than the repeatability limit *r* (reproducibility limit *R*).

Based on belonging to the same population (Student's t-test, method of control charts), it was observed that the flat specimens without inclination of lower end/axis could be attached to ID specimens to determine engineering limits. This significantly increases the number of specimens (e.g. N = 19 to N = 43), which is not irrelevant from the statistical and geotechnical viewpoint. Finally, engineering limits *LEL* and *UEL* were determined for all mechanical properties (see **Table 3**) according to the principle shown in **Figure 8**, with controlled probabilities of errors of the 1st and 2nd kind $\alpha, \beta \leq 10\%$.

### 3.1.2. Effects of flatness on mechanical properties

To investigate the impact of flatness, the research included 24 specimens of group B (flatness only, $R = W =$ 0.03–0.5 mm) and 23 specimens of group C (combined parallelism $P = \Delta\varphi =$ 0.5–2.3° and flatness $R = W =$ 0.04–0.3 mm). Specimen properties are presented in **Table 1**, the examples of *σ*-*ε* curves in Section 3.3 (together with energy curves), and the shortened results in **Table 2**. Y-shaped failure, local/multiple fracturing, longitudinal foliation, cracking and crushing of irregularities on the upper end characterise the conducted uniaxial tests for both groups B and C. This is also visible through improper 'toothed' diagrams with progressive irregularities and reduced *UCS*. Failure modes depend on the type of surface waviness: for convex Bkv/Ckv type pushing of upper 'cone' inside, longitudinal foliation outside, and local crushing of the remaining higher edge of the upper end is noticed; for the Bkk/Ckk type local fracture in the form of chamfered edge; and the Bmj/Cmj type, a combination of the previous two (see **Figure 7**).

Due to the non-flatness, significant decrease of mean values and increased variability (*s*, *Cv*) are present for all properties (see **Table 2**), except for moduli *E* and $E_{sg}$. At the highest *R*, *UCS* and $UCS_{50}$ drop to 40–50% of the reference *LEL* value. For $E_L$ and $E_{L,2}$, edges are included in the measurement of deformations, and flatness dependence is expected.

**Figures 9–11** depict the behaviour models for mechanical properties with *LEL*/*UEL* limits indicated; the critical flatness $R_{cr}$ is at the intersection of *LEL* and the presented diagrams.

According to the presented results, *for UCS*, *the critical flatness is* $R_{cr} = 0.08$ *mm* (on one specimen end), **Figures 9a** (at small *P* and *O*, group B) and **9c** (all specimens, N = 90). "Small *P* and *O*" here means $P < 0.5°$ and $O < 0.3°$, which results from wider considerations and analysis of groups A and D (values where there are

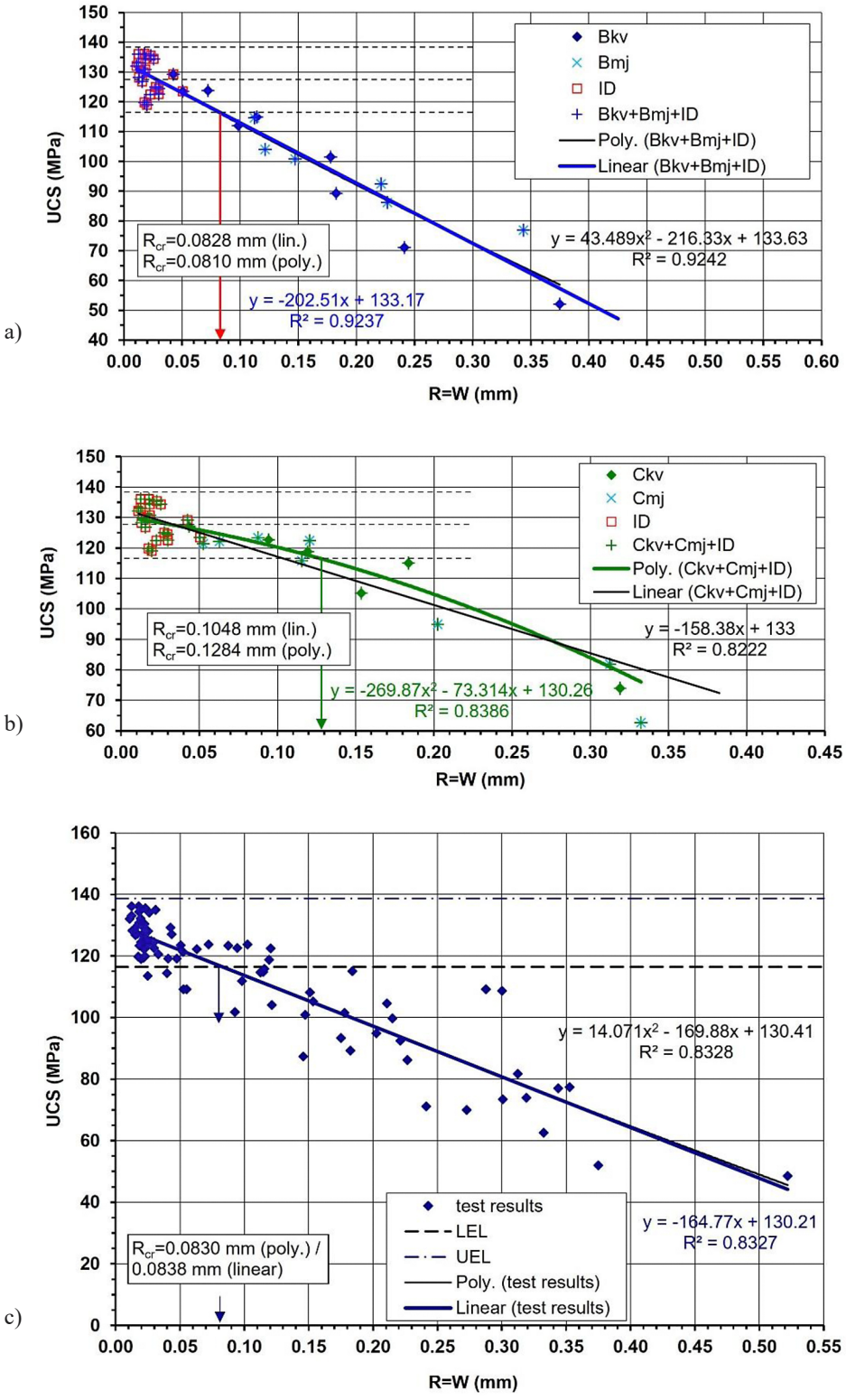


**Figure 9.** Relationship of flatness and uniaxial compressive strength: a) for specimens of Bkv and Bmj subgroups (realistic – convex and mixed profile types, at small *P* and *O*); b) for specimens of Ckv and Cmj subgroups (realistic non-flatness types, at small *O* and *P* > 0.5°); c) for all specimens (N = 90)

no unfavourable effects on *UCS*/*E*/*v*, as demonstrated in Section 3.1.3). Similar results and *the same conclusion apply to* $UCS_{50}$ (**Štambuk Cvitanović, 2012**).

The results of group C show that parallelism has no additional negative impact, i.e. it does not reduce $R_{cr}$ for *UCS* (see **Figure 9b**); the same is true for other mechanical properties (**Štambuk Cvitanović, 2012**), so the previous conclusions remain.

It is important to note that the concave type of surface profiles appear rarely in laboratory practice as a conse-

a)

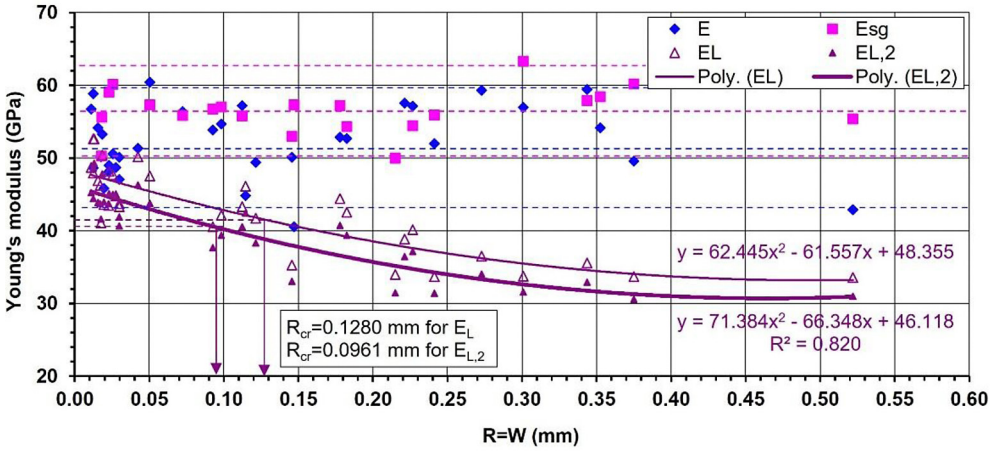


b)

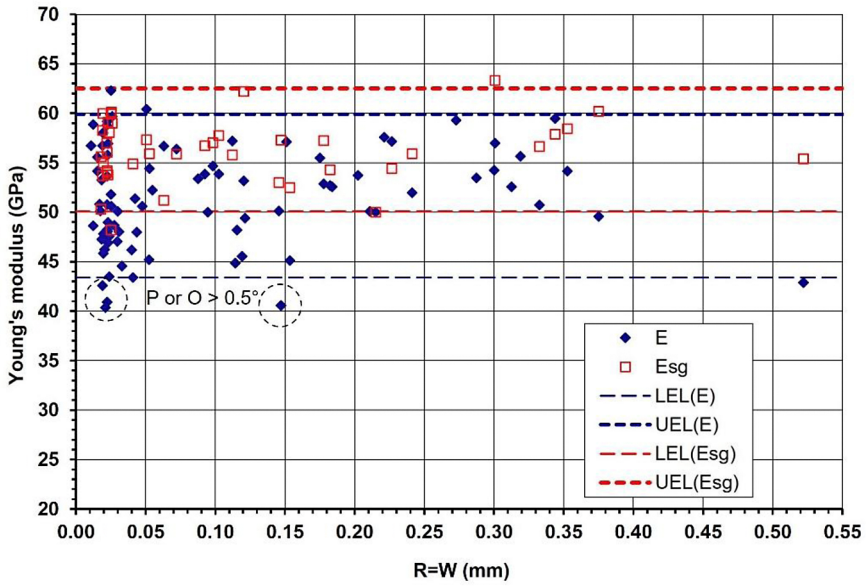


c)

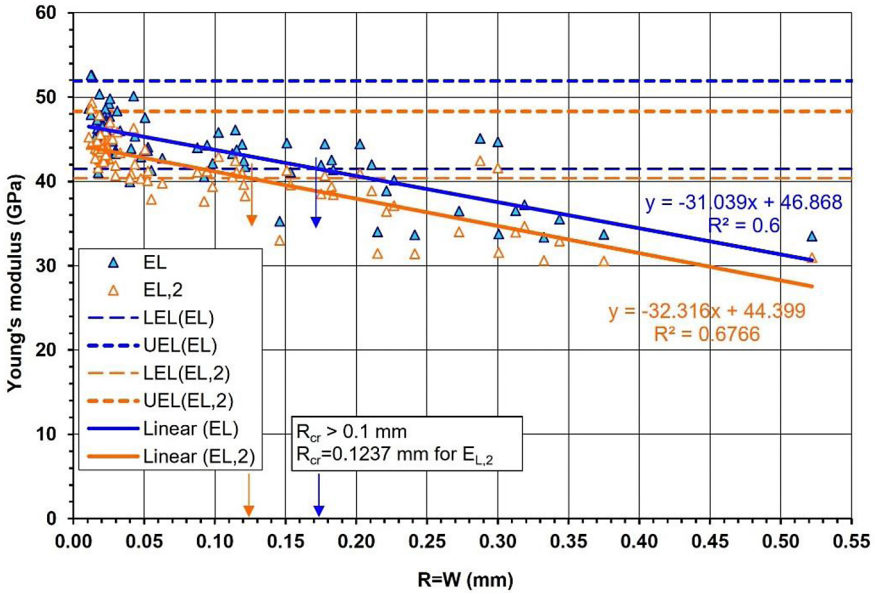


**Figure 10.** Relationship of flatness and Young's modulus: a) $E$, $E_{sg}$, $E_L$ and $E_{L,2}$ based on the results of group B (B + ID; N = 34 for $E$, $E_L$ and $E_{L,2}$; N = 21 for $E_{sg}$); b) $E$ and $E_{sg}$ for all specimens (N = 86 for $E$, N = 41 for $E_{sg}$); c) $E_L$ and $E_{L,2}$ for all specimens (N = 85)

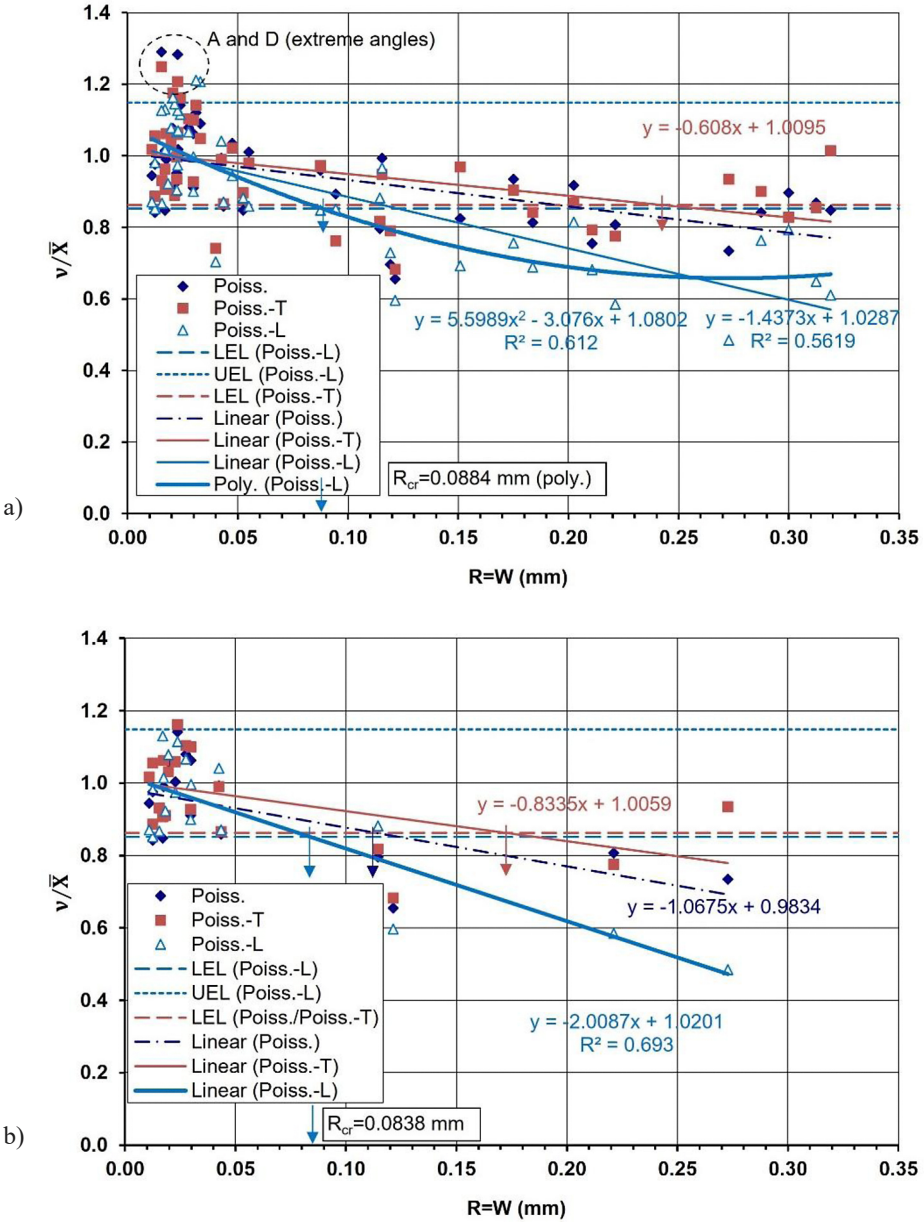


**Figure 11.** Relationship of flatness and normalised Poisson's ratio: a) for all specimens (N = 46); b) for specimens with small angle irregularities ($P < 0.5°$ and $O < 0.3°$, N = 19)

quence of the specimen preparation process. From many recorded samples, it was observed that cutting and grinding in laboratory conditions gave mostly convex and mixed profiles. Therefore, the results for realistic convex and mixed profiles are presented (see **Figures 9a** and **9b**); the concave subgroups Bkk and Ckk give similar results.

Young's moduli $E$ and $E_{sg}$ practically do not depend on the flatness $R$ (see **Figures 10a** and **10b**), unlike moduli $E_L$ and $E_{L,2}$, which decrease with increasing $R$ ($R_{cr} \geq 0.10$ mm; see **Figures 10a** and **10c**). If only specimens with small angular irregularities are selected in **Figure 10c**, the result is the same as in **Figure 10a**.

Poisson's ratio generally begins to fall when $R > 0.1$ mm ($v$, $v_T$), and *for* $v_L$, *the critical flatness is* $R_{cr} = 0.08$ *mm* (see **Figure 11**), the same as for *UCS*. For all other deformability parameters (Young's moduli and Poisson's ratios), it is reasonable to accept $R_{cr} = 0.1$ mm (on the one specimen end).

### 3.1.3. Effects of angular irregularities - parallelism and perpendicularity

To investigate the effects of angular shape irregularities, the testing programme included 24 specimens of group A (increasing parallelism in the range $P = \Delta\varphi =$ 0.2-2°) and 8 specimens of group D (increasing perpendicularity in the range $O = \varphi'' =$ 0.2-2.2°). Shape tolerances are presented in **Table 1**, examples of $\sigma$-$\varepsilon$ curves in Section 3.3 (together with energy curves), and shortened results in **Table 2**. During the testing of these flat sam-

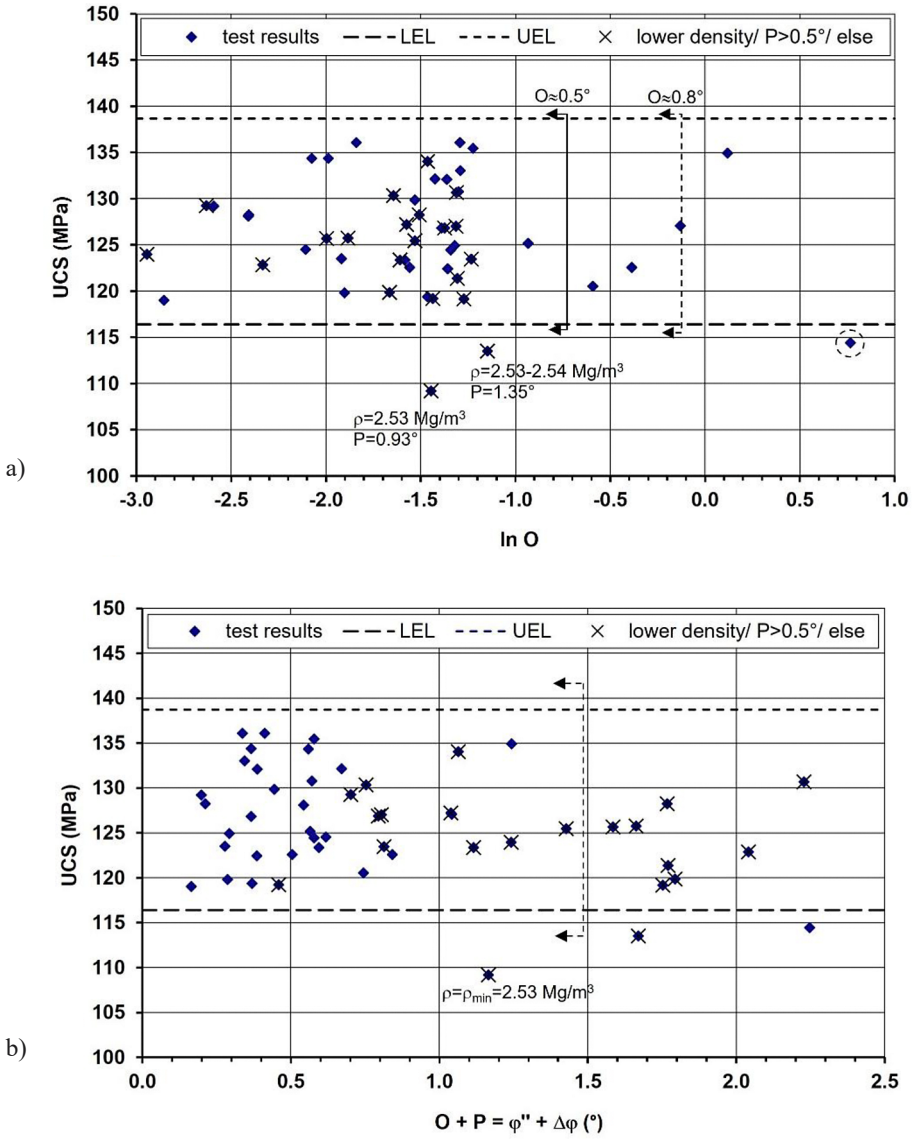


**Figure 12.** Relations of angular irregularities and *UCS* for all flat specimens ($R$ < 0.05 mm, N = 51): a) relation *UCS* – ln *O*; b) relation *UCS* – (*O* + *P*). Similar relationships apply to $UCS_{50}$.

ples, the self-adjusting joint enables the adjustment of the upper pressure plate to the inclination of the upper specimen end, with a smooth test flow and smooth $\sigma$-$\varepsilon$ curves. The influences on *UCS*/*E*/*v* are much less pronounced than with the previously described induced non-flatness, and the failure modes do not show the characteristics of local failures. Some failures are almost as in group ID, and there is also a separation of the lateral segments and longitudinal foliation in group A; group D is the same but with axial splitting of inclined to subvertical surfaces (see **Figure 7**). Behaviour models with *LEL*/*UEL* limits are shown in **Figures 12–14**.

The mean values of *UCS*/*E*/*v* (groups A and D in **Table 2**) do not differ from the reference ones in **Table 3**, except for a slight increase in $v_L$ (< 10%) and a decrease in *E* in group D (by 13%, almost the same value as $E_L$). Statistical properties *s* and *Cv* are generally better or close to the properties of specimens without shape irregularities from the ASTM study (see **Table 3**), except for Poisson's ratio in general and *E* in group A.

As shown in **Figure 12**, *UCS* and $UCS_{50}$ in a practical sense do not depend on either *O* or sum *O* + *P* (therefore, they do not depend on *P* either, as shown in section 3.3 and in **Štambuk Cvitanović, 2012, 2015b**). There is no correlation. The values only vary between the *LEL* and *UEL* limits, especially when specimens with pronounced *P* (*P* > 0.5°) are excluded, i.e. realistic samples taken. The same applies to Young's modulus (see **Figure 13**), where the perpendicularity is expressed as the relative deviation of coaxial alignment or concentricity of the specimen axis $|P_o/D|$.

Previous diagrams show reasonably narrower and wider limits of angular irregularities for strengths and moduli (*O* = 0.5° and 0.8°; and the same is true for *P*),

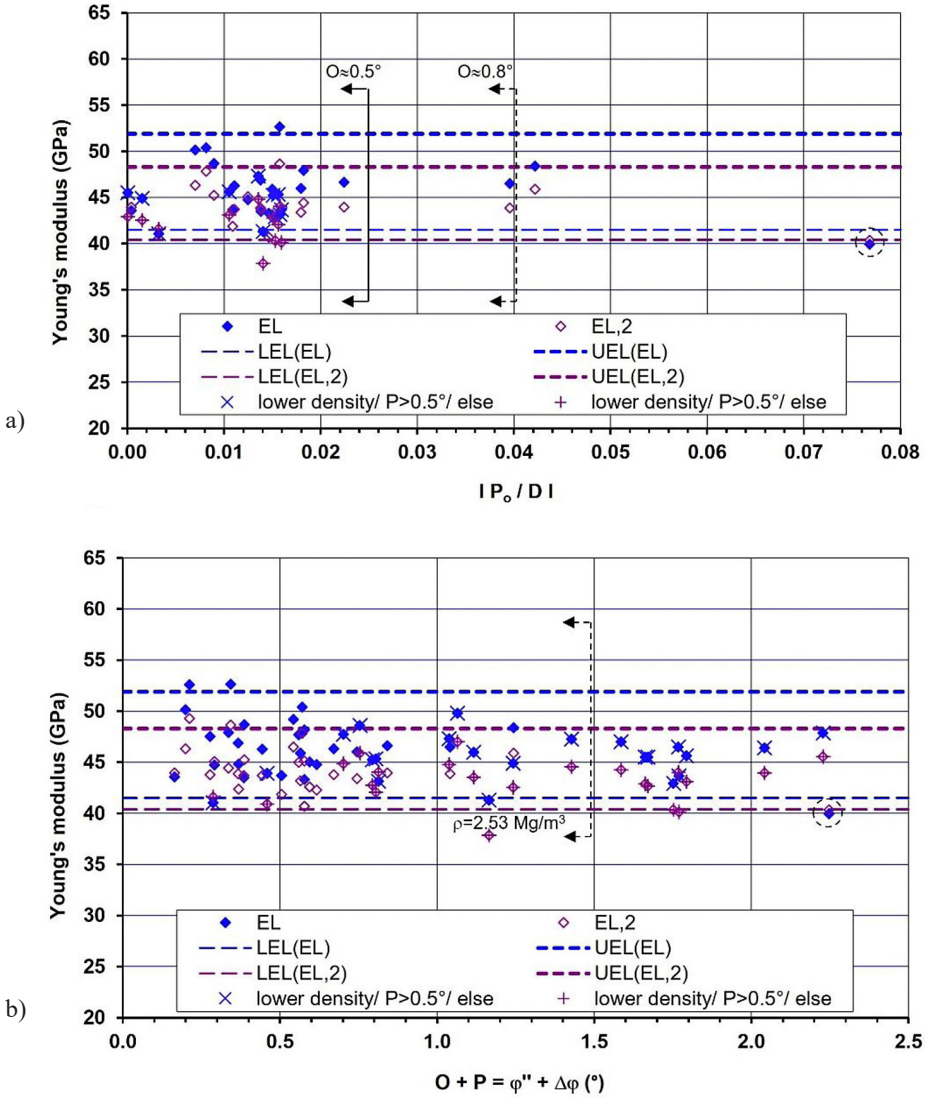


**Figure 13.** Relations of angular irregularities and Young's modulus for flat specimens:
a) relation of moduli $E_L$ and $E_{L,2}$ and perpendicularity (as $|P_o/D|$) (N = 29 for specimens with measured $P_o$);
b) relation of moduli $E_L$ and $E_{L,2}$ and sum ($O + P$) (N = 48). Similar relationships apply to $E$ and $E_{sg}$.

where the wider limit was chosen as such due to the smaller number of results. Also, according to the obtained results, for all strengths and moduli, it is reasonable to limit the sum ($O + P$) to 1.5°.

Poisson's ratio is the mechanical property most sensitive to angular irregularities (more dependent on $O$ than $P$). **Figures 14a** and **14b** show the ranges of normalised Poisson's ratio $v_T/\overline{X}$ and $v_L/\overline{X}$ (where $\overline{X}$ is the mean value from **Table 3**) for each specimen when $v_T$ and $v_L$ are calculated for varying stress increments $\Delta\sigma$ = 40–60%, 42.5–57.5% and 45–55% of *UCS*. In **Figure 14a**, marked specimens with $O$ above 0.25° and $P_o > 0.7$ mm/$P_c > 0.6$ mm exceed *LEL*/*UEL*. However, without such specimens, $P$ can increase up to about 1.5°. If group D with extreme $O$ is excluded, for the marked specimens with $O$ < 0.3° in groups A and $C_{0.05}$ (flat C specimens), critical values appear at $P > 0.5°$.

As shown in **Figure 14b**, for small $P$ up to 0.5°, $|P_o/D|$ can increase to about 3% (the corresponding $O$ is about 0.5° or a little more), while for the largest $P$ (groups A and C) $|P_o/D|$ should be limited to 1.5% ($O$ to 0.3°). Based on the observation of the sum of angles of $O$ and $P$ (see **Figure 14c**), unfavourable effects on $v$ occur at $(O + P) \geq 0.8°$.

Therefore, for $O$ to 0.25°, Poisson's ratio in a practical sense does not depend on $P$ (max $P$ = 1.5°), and for $O$ to 0.5° (recommendation 0.3°), $P$ to 0.5° and ($O + P$) to 0.8° unfavourable impacts to Poisson's ratio will not appear.

### 3.2. Results verification - statistical and numerical models

To identify any new connection of input/output variables and assess the results of natural models, the research

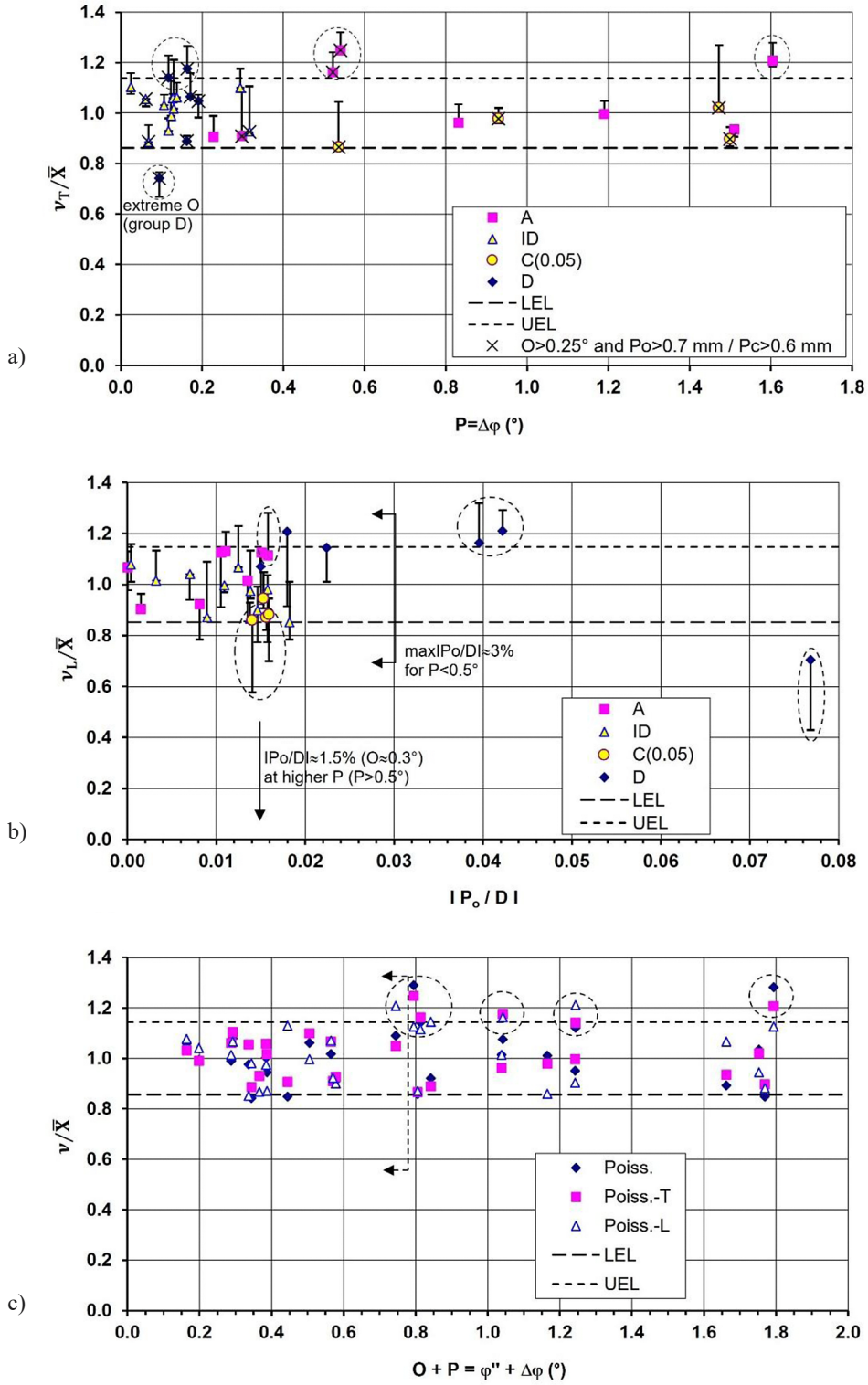


**Figure 14.** Relations of angular irregularities and Poisson's ratio for flat specimens (N = 29): a) relation of normalised Poisson's ratio $v_T$ and parallelism $P$; b) relation of normalised Poisson's ratio $v_L$ and perpendicularity $O$ (as $|P_o/D|$); c) relation of normalised Poisson's ratio ($v$, $v_T$, $v_L$) and sum ($O + P$)

included additional analysis of the results using Response Surface Methodology (RSM) and multiple regression. According to all the obtained results, *UCS*, $UCS_{50}$ and $v_L$ are the mechanical properties with the greatest changes due to shape tolerances. Statistical models (nine models for $UCS/UCS_{50}$ and three for $v_L$) were developed for these properties, as described in **Štambuk Cvitanović (2012)** and **Štambuk Cvitanović et al. (2015a)**.

**Figure 15** provides previously unshown examples of the obtained models for the *UCS* (as $UCS_{50}$) and $v_L$,

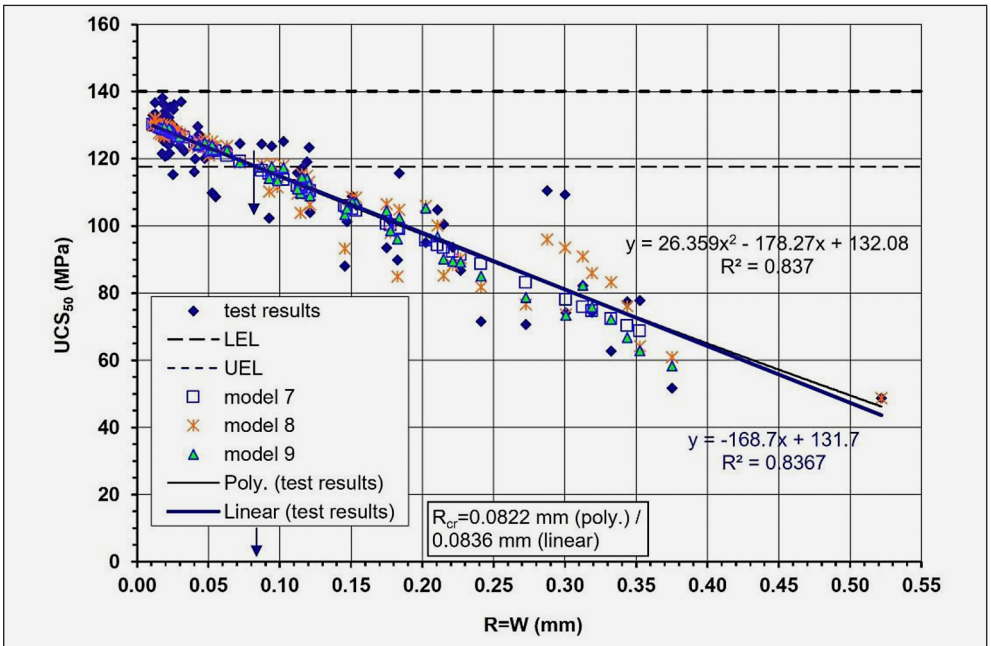


Model 7: $UCS_{50}/\bar{X} = 1.0262 - 1.3989\ R$
Model 8: $UCS_{50}/\bar{X} = 0.3448 + 0.0870\ \ln P - 0.3503\ \ln R + 0.0244\ \ln R\ \ln P - 0.0474\ (\ln R)^2$
Model 9: $UCS_{50}/\bar{X} = 1.0260 - 1.5449\ R + 0.2272\ R\ P$

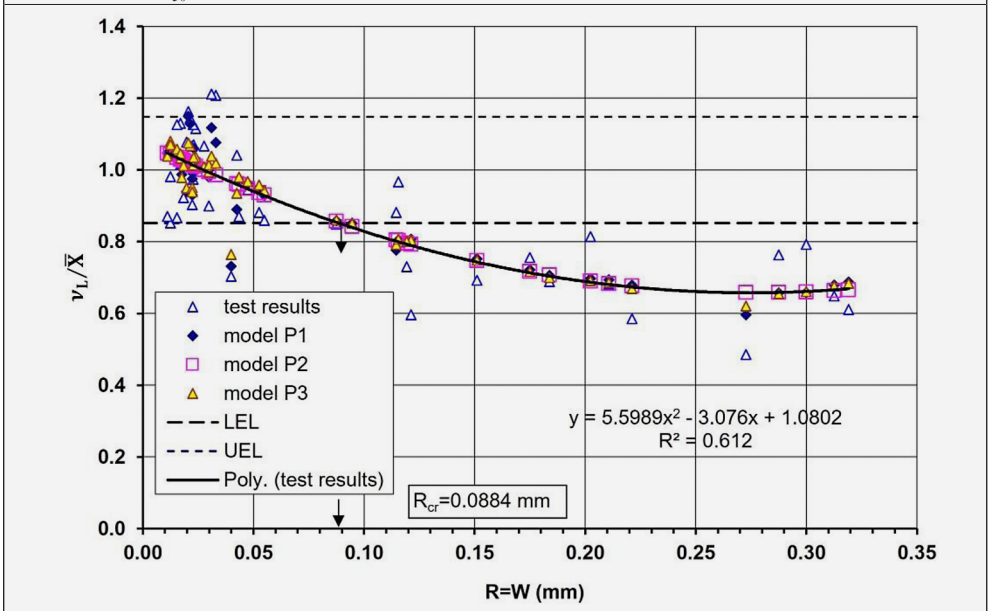


Model P1: $v_L/\bar{X} = 0.9658 - 2.8451\ R + 0.5033\ O + 4.9736\ R^2 - 0.2617\ O^2$
Model P2: $v_L/\bar{X} = 1.0798 - 3.0205\ R + 5.4034\ R^2$
Model P3: $v_L/\bar{X} = 1.0070 - 3.2037\ R + 8.5698\ |P_o/D| + 5.8538\ R^2 - 132.6015\ |P_o/D|^2$

**Figure 15.** Examples of statistical models: a) relation of $UCS_{50}$ and $R$ (all specimens, N = 90); b) relation of normalised Poisson's ratio $v_L/\bar{X}$ and $R$ (N = 46); $\bar{X}$ is the mean value from **Table 3**

where $R_{cr}$ remains unchanged. According to the results of the RSM, for $UCS/UCS_{50}$, the variables $R$ and $P$ (and not $O$) are statistically significant, where $P$ is significant only at higher $R$. At the same time, for $v_L$, only $R$ and $O$ (or $|P_o/D|$) are statistically significant (without $P$). This finding is consistent with the natural models.

The research also included a comparison of the results related to $UCS$ with the numerical model based on the Embedded Discontinuity Finite Element Method (ED-FEM), where substantial agreement was obtained between the experimental and numerical results (**Štambuk Cvitanović et al., 2015b**).

### 3.3. Energy approach

To study the effects of shape tolerances on energy dissipation properties as indicators of changes and progressive damage/failure during uniaxial testing, the analysis included the determination of total $W_t$, elastic $W_e$ and dis-

**Table 4.** Summary of the results related to energy dissipation properties

| Group, property | | Point 1-CP | | | | Point 2-YP | | | | Point 3-*UCS* | | | | Region 3-4 | | |
|---|---|---|---|---|---|---|---|---|---|---|---|---|---|---|---|---|
| | | $\lambda_1$ | $W_{t1}$ | $W_{e1}$ | $W_{d1}$ | $\lambda_2$ | $W_{t2}$ | $W_{e2}$ | $W_{d2}$ | $\lambda_3$ | $W_{t3}$ | $W_{e3}$ | $W_{d3}$ | $\lambda_{3\text{-}4}$ | $W_{tmax}$ | $W_{dmax}$ |
| | | | (kJ/m³) | | | | (kJ/m³) | | | | (kJ/m³) | | | | (kJ/m³) | |
| **ID** as ID-o | *Min* | 2.10 | 0.007 | 0.002 | 0.005 | -0.028 | 33.6 | 34.5 | -0.960 | 0.299 | 202.9 | 148.6 | 46.7 | 1.70 | 224.0 | 139.9 |
| | *Max* | 4.0 | 0.037 | 0.010 | 0.027 | 0.114 | 157.3 | 141.3 | 16.0 | 0.706 | 310.3 | 181.9 | 128.4 | >10⁵ | 684.2 | 683.0 |
| | $\bar{X}$ | 3.29 | 0.016 | 0.004 | 0.012 | 0.036 | 78.5 | 74.5 | 3.98 | 0.484 | 236.6 | 158.7 | 77.9 | >10⁴ | 373.0 | 330.3 |
| | *LEL* | - | - | - | - | - | - | - | - | - | 156.8 | 135.2 | - | - | - | - |
| | *UEL* | - | - | - | - | - | - | - | - | - | 316.4 | 182.2 | - | - | - | - |
| A | *Min* | 1.64 | 0.008 | 0.002 | 0.005 | -0.015 | 6.70 | 6.81 | -0.286 | 0.259 | 165.8 | 128.8 | 34.1 | 0.488 | 183.6 | 58.9 |
| | *Max* | 7.29 | 0.017 | 0.003 | 0.015 | 0.089 | 113.6 | 104.7 | 9.10 | 1.03 | 317.2 | 162.2 | 160.7 | >10⁵ | 602.9 | 556.3 |
| | $\bar{X}$ | 3.74 | 0.012 | 0.003 | 0.010 | 0.030 | 72.5 | 69.4 | 3.09 | 0.585 | 237.2 | 149.0 | 88.2 | >10⁴ | 338.4 | 246.0 |
| | $\boldsymbol{P_{cr}}$ **(°)** | - | - | - | - | - | **1.9** | **1.9** | - | **1.9** | **0.8** | **1.0 - 1.5** | **0.5** | **0.5** | - | **0.8** |
| B | *Min* | 0.670 | 0.007 | 0.002 | 0.004 | -0.495 | 4.37 | 8.67 | -4.29 | 0.108 | 40.4 | 27.3 | 6.70 | 0.634 | 81.0 | 44.4 |
| | *Max* | 5.31 | 0.053 | 0.032 | 0.021 | 0.126 | 135.9 | 123.8 | 15.2 | 4.99 | 283.0 | 147.0 | 235.8 | ≈10⁵ | 494.4 | 494.4 |
| | $\bar{X}$ | 3.49 | 0.017 | 0.006 | 0.012 | -0.005 | 57.5 | 55.0 | 2.46 | 0.815 | 133.0 | 83.3 | 49.7 | >10⁴ | 279.5 | 244.8 |
| | $\boldsymbol{R_{cr}}$ **(mm)** | **0.1** | **0.3** | **0.3** | - | **0.3** | **0.2** | **0.2** | **0.3** | **0.08 - 0.1** | **0.08** | **0.08** | **0.08 - 0.1** | **0.08** | **0.08** | **0.08** |
| C | *Min* | 1.12 | 0.012 | 0.002 | 0.010 | 0.004 | 18.9 | 18.3 | 0.168 | 0.065 | 40.2 | 36.8 | 3.42 | 0.474 | 52.3 | 22.6 |
| | *Max* | 12.8 | 0.037 | 0.011 | 0.034 | 0.065 | 112.1 | 105.2 | 6.85 | 0.464 | 208.5 | 150.4 | 61.1 | 325.6 | 402.4 | 333.0 |
| | $\bar{X}$ | 4.16 | 0.020 | 0.005 | 0.015 | 0.025 | 64.7 | 62.9 | 1.82 | 0.236 | 139.6 | 110.3 | 29.3 | 53.7 | 251.3 | 188.0 |
| | $\boldsymbol{R_{cr}}$ **(mm)** | **0.1 - 0.2** | - | **0.1** | **0.1** | - | **0.3** | **0.3** | **0.1** | **0.2** | **0.1 - 0.2** | **0.1** | **0.1** | **0.1 - 0.2** | **0.1 - 0.2** | **0.1 - 0.2** |
| D | *Min* | 2.06 | 0.011 | 0.002 | 0.009 | 0.009 | 36.0 | 35.0 | 0.753 | 0.192 | 164.2 | 112.5 | 31.3 | 0.194 | 173.6 | 31.6 |
| | *Max* | 7.67 | 0.030 | 0.007 | 0.023 | 0.058 | 153.6 | 145.1 | 8.45 | 0.825 | 298.7 | 189.5 | 135.1 | 73.2 | 444.8 | 542.1 |
| | $\bar{X}$ | 5.20 | 0.016 | 0.003 | 0.013 | 0.030 | 99.9 | 96.8 | 3.13 | 0.387 | 224.3 | 162.3 | 62.0 | 11.0 | 278.7 | 222.7 |
| | $\boldsymbol{O_{cr}}$ **(°)** | **0.3 - 0.4** | - | - | - | - | - | - | - | **0.5** | - | **0.7** | **0.5** | **0.5** | - | **0.5** |

Gray - decrease in value of 20% or more; underlined - increase in value of 20% or more
Region 3-4 = post-failure region of the stress-strain curve; $W_{emax} = W_{e3}$ (not double-specified)
These results included 50 samples and 70 stress-strain curves with strains determined by LVDTs and/or strain gauges.
$W_{d2}$ and $\lambda_2$ sometimes appear as apparent small negative values due to the non-linearity of the $\sigma$-$\varepsilon$ curve or 'toothed' diagrams (calculation of $W_e$ from $E$; the difference between the current modulus value and the "average" $E$).
To determine *LEL* and *UEL* ($W_{t3}$, $W_{e3}$), the measurement uncertainty ($U = 2s$) was applied as a generally accepted measure of dispersion. Due to the high variability of energy indicators, such analyses did not apply to other parameters, and the min and max values of the ID group were taken, which gives narrower limits.

sipated energy $W_d$, as well as the energy dissipation coefficient $\lambda = W_d/W_e$ at three characteristic $\sigma$-$\varepsilon$ points: 1-CP closure point, 2-YP yield point, and 3-*UCS*/peak point (see **Figure 1**, **Equations 12–15**, **Table 4**).

In addition to the $\sigma$-$\varepsilon$ curve, the energy approach also describes the process of rock deformation and failure (**Gong et al., 2019; He et al., 2020; Liu et al., 2019; Taheri et al., 2016**), which is characterised by the following four phases:

1. During the *compaction* phase (from point 0 to 1-CP in **Figure 1**), the microcracks are closing, followed by an increase in energy with stress, mostly dissipated ($W_d$ dominates because considerable energy is dissipated during the closing of cracks and pores) and a strong growth of $\lambda$ up to the value $\lambda_1$.

2. In the *elastic* phase (from 1-CP to 2-YP), $W_t$ and $W_e$ grow linearly with stress, generating considerable energy and transforming into elastic strain ($W_e$ predominates), reaching a maximum $W_e$ growth rate. At the same time, $W_d$ is relatively low and stable (no propagation of new cracks) and $\lambda$ decreases and reaches a minimum $\lambda_2$ at point 2-YP.

3. In the *yield* phase (from 2-YP to 3-*UCS*), $W_t$ continues to grow, but in decreasing increments, as well as $W_e$ (which still dominates in relation to $W_d$). Crack generation and propagation begin, and $W_e$ reaches a maximum at the peak point 3-*UCS*. This phase is characterised by a strong growth of $W_d$, while $\lambda$ also grows (but slightly) due to the increase in microcracks.

4. Finally, in the *failure* phase, when strength is reached at point 3-*UCS*, macroscopic breakdown of the

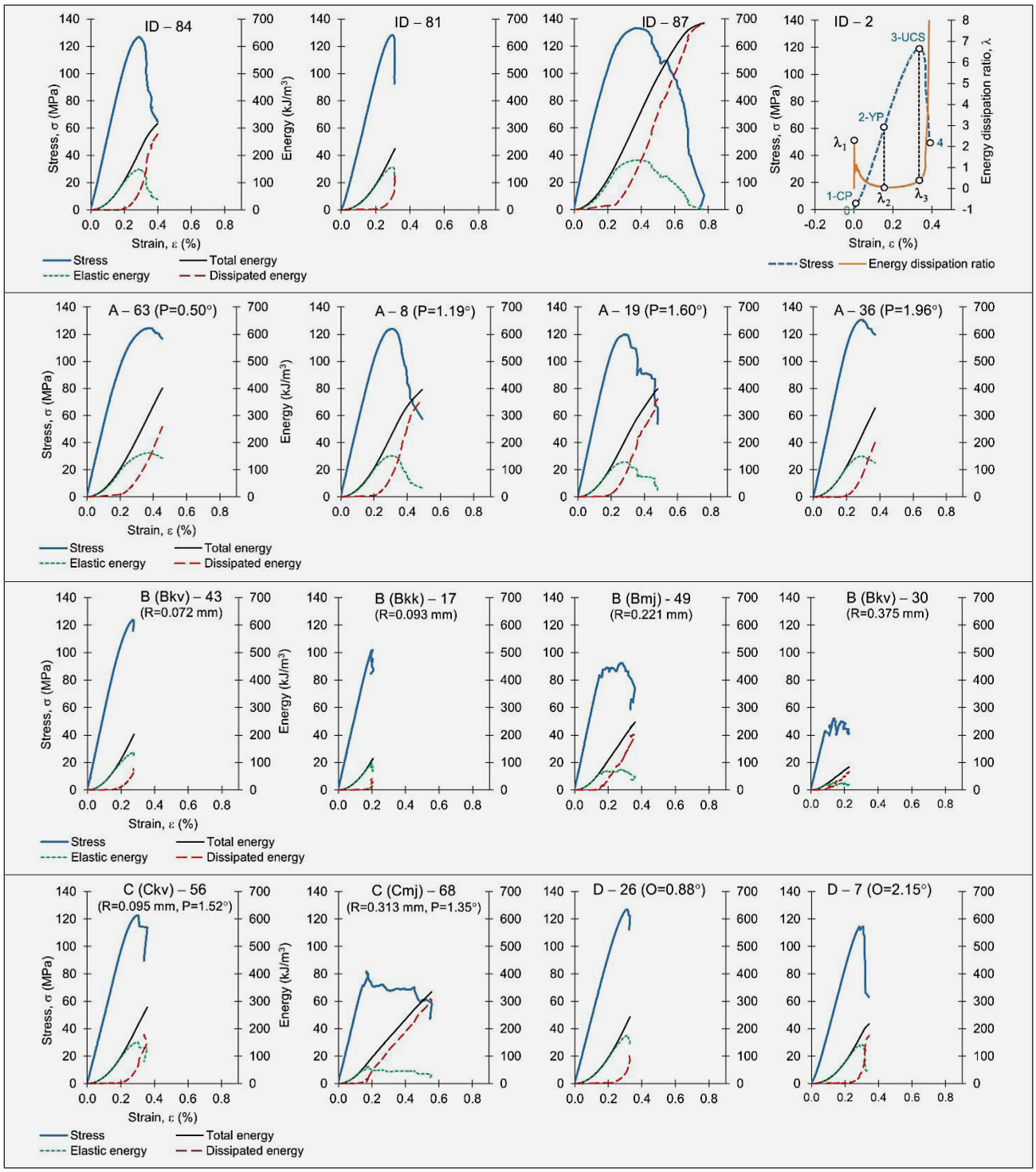


**Figure 16.** Examples of total, elastic, and dissipated energy curves by groups of specimens, shown together with σ-ε curves for increasing levels of shape irregularities. The diagram for specimen 2 from group ID (ID - 2, top row, right) shows the typical (N-shaped) change in $\lambda$ during uniaxial testing.

specimen occurs with the rapid expansion of internal cracks and strong release of $W_e$ accumulated in the specimen (transformation into $W_d$). At the same time, $W_d$ grows quickly and exceeds $W_e$ ($W_d$ dominates). The growth of $W_d$ is accompanied by a steep increase in $\lambda$ due to the constant release of $W_e$ and accelerated propagation of cracks, i.e. greater sliding between particles.

The described energy accumulation/dissipation process is obvious for specimens from the ID group, but in other groups with large *R*/*P*/*O* disturbances or changes in energy indicators occur in some or all described phases/points of the σ-ε curve (see **Figure 16**).

Through changes in energy indicators $W_{ti}$, $W_{ei}$, $W_{di}$, $\lambda_i$ (i = 1, 2, 3), which correspond to changes in the σ-ε rela-

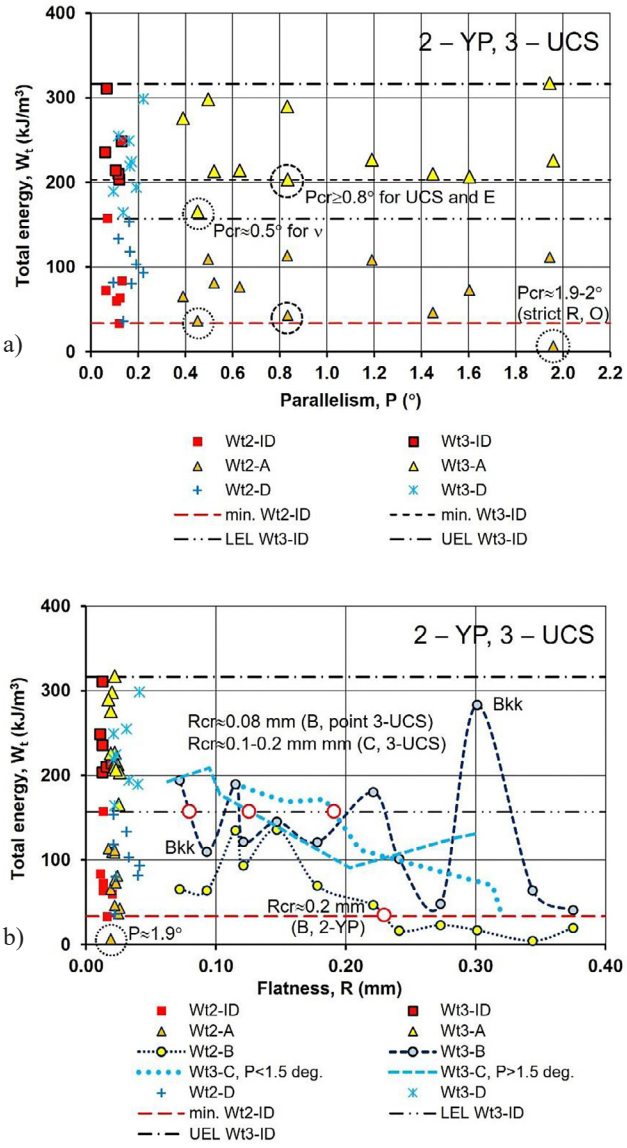


**Figure 17.** Total energy vs parallelism a) and flatness b)

tionship, it is possible to determine the critical values of shape tolerances $R_{cr}/P_{cr}/O_{cr}$ in a similar way as in natural models. This is shown in **Table 4** and **Figure 17**, where we applied the criterion of a change in energy indicators of 20% compared to the ID group (corresponding to the natural variability of mechanical properties from **Table 3**) and obtained almost the same values of $R_{cr}/P_{cr}/O_{cr}$ as with the previous natural, statistical and numerical models.

In **Figure 17a**, with an increase in $P$ up to 2°, no significant decrease in $W_t$ was generally registered, neither in point 2-YP nor in point 3-*UCS*. This confirms that strength and moduli in a practical sense do not depend on $P$ for spherically seated test machines, and that is also described by natural models. According to natural models (see **Figure 14**), $P_{cr}$ = 0.5° refers to Poisson's ratio (then it also applies to Young's modulus determined simultaneously), and $P_{cr}$ = 0.8° to all strength and moduli when there is no need to measure Poisson's ratio.

Regarding the influence of flatness on energy indicators, an example of the $W_t$ results is shown in **Figure 17b**; similar results were obtained for $W_e$ and $W_d$. Consistent with previous results (see **Figures 9–11**), criterion $R_{cr}$ = 0.08 mm refers to *UCS* (or $UCS_{50}$) and $v_L$, and $R_{cr} \geq 0.1$ mm (reasonable limitation $R_{cr}$ = 0.1 mm) to all other mechanical properties. Since it is impossible to present all the results here, an overview of the main results is provided in **Table 4**.

## 4. Discussion

In this paper, we have presented the results of extensive research on 90 rock core specimens, which established behaviour models for the mechanical properties *UCS*/*E*/*ν* depending on the specimen shape tolerances – flatness *R*, parallelism *P* and perpendicularity *O*. The related energy dissipation properties were also included in the research. Based on all findings and the limits of the natural variability of limestone rock, we determined the critical values of shape tolerances $R_{cr}/P_{cr}/O_{cr}$ at which there will be no negative effects on the mechanical properties.

**Figures 18** and **19** compare the results obtained here and the previous results (**Hoskins and Horino, 1968**) that determined the current tolerances. The figures show that the results of this study fit well, with a significant improvement in the coverage range and the number of specimens, i.e. a better characterisation of the influence of *R* and *P* on *UCS*.

Furthermore, the analysis of the results obtained by CMS on specimens produced without grinding (only with a saw cut) under laboratory conditions has shown that the flatness of such specimens is up to 0.2 mm. If this is compared with the critical flatness of $R_{cr}$ = 0.08 mm determined here, it can be concluded that grinding of the test specimens is necessary (as also reported by **Arzúa et al., 2020**).

As a result of considering all the results achieved and presented, suitable specimen shape tolerances were established for rocks of medium strength, taking into account the mechanical properties to be determined and the equipment set up for measuring the deformations. A comparative overview of the current ASTM/ISRM tolerances and the tolerances proposed in this study are shown in **Table 5**.

Other research that addresses the specimen characteristics focused mainly on other scale, end and shape effects, failure modes and different sources of *UCS*/*E*/*ν* variability (e.g. **Zhang et al., 2011; Liang et al., 2016; Zou and Wong, 2016; Gao et al., 2018; Du et al., 2019; Chen et al., 2020; Dong et al., 2021; Vaneghi et al., 2021**).

Recently, soft computation techniques have been proposed for predicting *UCS* (**Xie et al., 2024**). However, their disadvantage is that large datasets must be trained, and rock properties vary locally, leading to direct testing of *UCS* as an output parameter. Few studies address the

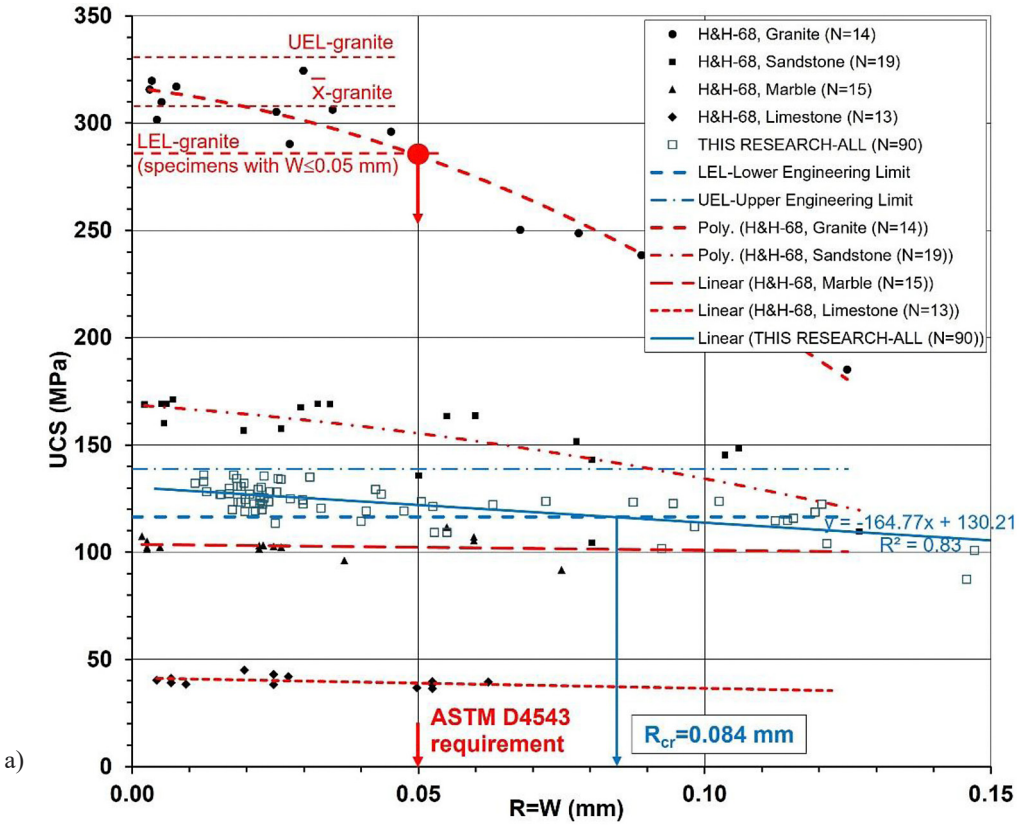


a)

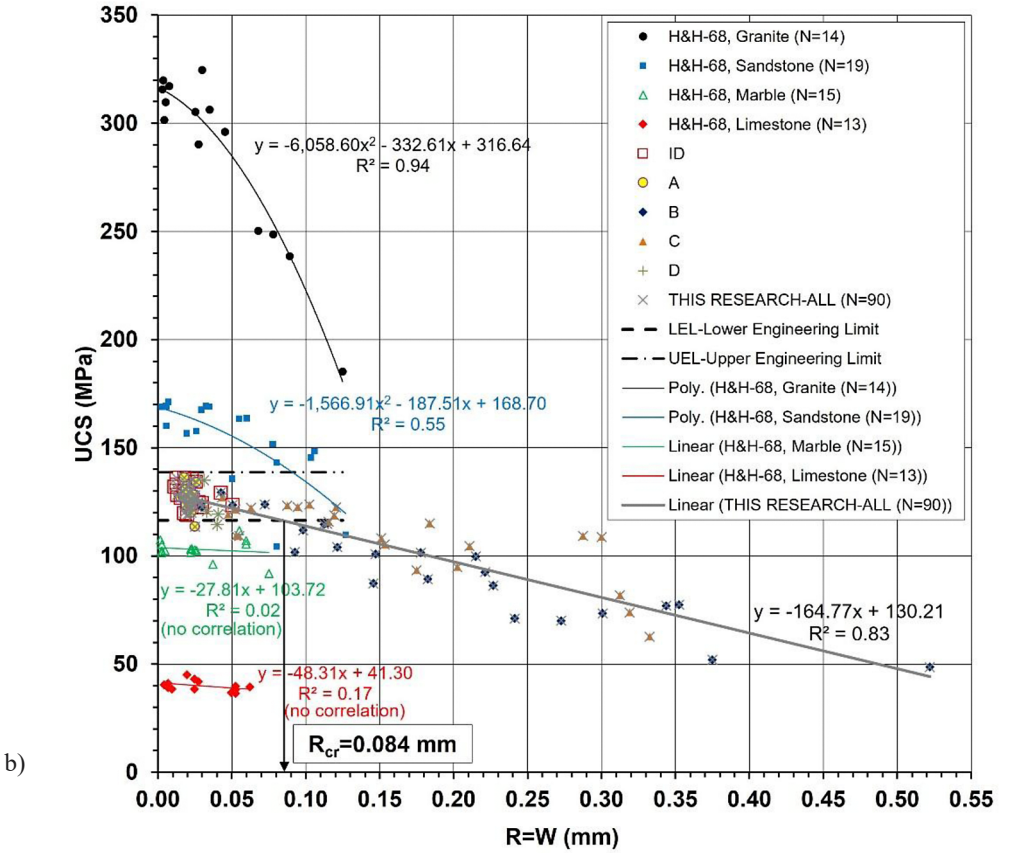


b)

**Figure 18.** *UCS* vs flatness: the results of this research compared to previously known results (recalculated to SI units); a) narrow $R = W$ range; b) wider $R = W$ range

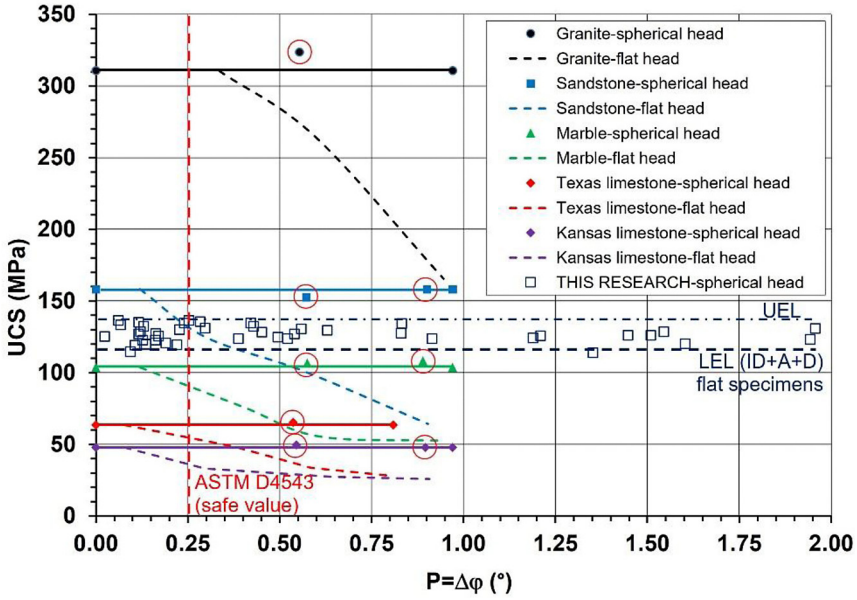


**Figure 19.** *UCS* vs parellelism: results of this research compared to previously known results (*UCS* recalculated to SI units)

**Table 5.** Review of current and newly proposed specimen shape tolerances

| SPECIMEN SHAPE TOLERANCE | ASTM (ASTM D4543-19) | ISRM (ISRM, 1979; 1983; 1999; 2007) | THIS RESEARCH (proposal of the new tolerances) |
|---|---|---|---|
| End flatness<br>$R = W \approx 2\delta$ | 0.05 mm<br>(valid for both ends) | 0.02 mm<br>(valid for both ends) | 0.08 mm for *UCS* ($UCS_{50}$)<br>0.08 mm for $v_L$, recommendation 0.05 mm<br>0.10 mm other properties (in line with *UCS*)<br>on the one end; total for both ends:<br>0.08 + 0.05 = 0.13 or 0.10 + 0.05 = 0.15 mm |
| Perpendicularity<br>$O = \varphi$" | 0.25°<br>(both ends) | 0.057°<br>or 0.05 in 50 mm<br>(both ends) | 0.3° recommendation for Poisson's ratio<br>0.5° general (i) (ii) (iii)<br>0.8° expanded, for strength and moduli (iv)<br>(*O* is linked to the lower end) |
| Parallelism<br>$P = \Delta\varphi$ | 0.25°<br>(spherically seated test machines) | 2×0.057 = 0.11°<br>or 0.10 in 50 mm<br>(indirectly) | 1.0° for *UCS* ($UCS_{50}$) and $E_L$ ($E_{L\,2}$) (i)<br>0.5° for Poisson's ratio and $E$, $E_{sg}$ (ii)<br>0.8° general for strength and moduli (iii) |
| Perpendicularity and parallelism<br>($O + P$) | 3×0.25 = 0.75°<br>(indirectly) | 3×0.057 = 0.17°<br>or 0.150 in 50 mm<br>(indirectly) | None (no correlation) (i) (iii)<br>0.8° for Poisson's ratio and $E$, $E_{sg}$ (ii)<br>1.5° expanded, for strength and moduli (iv) |
| Side straightness<br>$\Delta$ | 0.5 mm | 0.3 mm | 0.5 mm,<br>or (in combination with *O* and *L*) so that $\lvert Po/D \rvert$ to 0.04 (0.03 for Poisson's ratio) |

(i) when determining the strength and/or approximate modulus (deformations measured on the entire specimen length)
(ii) always when the Poisson's ratio will be tested, or when Young's modulus and Poisson's ratio will be tested together by measuring deformations in the middle of the specimen (deformability in general)
(iii) general criterion for all the strength and moduli when there is no need to measure Poisson's ratio
(iv) a smaller number of test results (observed properties are still within engineering limits)

influence of tolerances, and no studies have been found that would be fully applicable in optimizing or upgrading specimen preparation requirements. This is supported by the fact that there are no new results in the standards and documents for application.

## 5. Conclusions

The main conclusions from the all modelling and energy analyses are listed below.

1. *Dependence on R of practical importance is registered (only) for the mechanical properties UCS, $UCS_{50}$ and $v_L$, with critical flatness $R_{cr}$ = 0.08 mm.* This flatness tolerance, obtained and appropriate for the considered medium-strength rock category, represents a decrease of current ASTM/ISRM requests.

2. The new $R_{cr}/P_{cr}/O_{cr}$ values shown in **Table 5** are proposed as an addition to the current ASTM/ISRM tolerances for the case of limestone or comparable medium-strength rock with *UCS* around 100–150 MPa. For

rocks with a lower *UCS*, these results are also valid. According to all previously obtained and presented results and **Table 5**, the starting hypothesis is supported.

3. Conducted research provides behaviour models for the influence of *R*/*P*/*O* on *UCS*/*E*/*v*, and the acceptance limits can then be set at will. Limits applied here reflect natural dispersion and variability under ideal (strict standardised) test conditions.

4. According to the obtained critical flatness $R_{cr}$ = 0.08 mm and the flatness of specimens prepared without grinding (up to 0.2 mm recorded by CMS in laboratory conditions), as a rule, it is necessary to grind the ends of the specimen.

5. For modern test machines with spherically seated upper platen (adjustment ability to 3°), in the flatness domain of interest ($R < 0.1$ mm), strength and moduli are independent of parallelism until about 1° or more.

6. With strict *O*, *P* can increase up to 1° (or more) without negatively impacting *v*, and vice versa. However, if one angle irregularity deviates, the other (or both) must be limited (see **Table 5**).

7. Moduli determined with deformations measured in the mid-height of the specimen practically do not depend on flatness, and measurements with strain gauges are particularly stable.

8. In the case of the new proposed models and tolerances, specimen preparation and verification procedures are facilitated. Namely, knowing the behaviour models obtained here, i.e. the severity of the consequences on the mechanical properties that will occur due to a certain level of shape tolerances, it is possible to make correct decisions on the acceptability/unacceptability of a particular specimen. That is, some specimens maybe do not have to be discarded or sent for repeated preparing, which depends on engineering judgment required by current standards in cases where it is not possible to achieve 'ideal' specimens. At the same time, the impact of shape deviations is known and controlled in the testing. The above ensures further positive effects in geotechnical projects (increasing the number of available samples, time and costs savings).

Finally, the aim of the research was fully achieved: to facilitate engineering judgement of rock specimen acceptance, especially when the number of available samples is small or the strict requirements of the standards cannot be achieved due to rock type/condition – to control and optimise rock strength and deformability testing for the case of 'medium' rock strength category (around 100–150 MPa).

### *Acknowledgement*

This research is partially supported through project KK.01.1.1.02.0027, a project co-financed by the Croatian Government and the European Union through the European Regional Development Fund - the Competitiveness and Cohesion Operational Programme. It is also supported through institutional projects GFV-IP-2024/25, Faculty of Geotechnical Engineering, University of Zagreb, Hallerova aleja 7, Varaždin (42000), Croatia. The authors are deeply grateful for this support.

## 5. References

Arzúa, J., Gonzáles, J., Erazo, I.T., Cánovas, M. and Alejano, L.R. (2020). Grinding or not grinding, that is the question. In: da Fontoura, S.A.B., Rocca, R.J. and Pavón Mendoza, J.F. (eds.): Rock Mechanics for Natural Resources and Infrastructure Development - Proceedings of the 14th International Congress on Rock Mechanics and Rock Engineering (ISRM 2019). CRC Press/Balkema, Leiden, The Netherlands, 2195-2202.

ASTM D4543-19 (2019). Standard practices for preparing rock core as cylindrical test specimens and verifying conformance to dimensional and shape tolerances, ASTM International, West Conshohocken, PA, USA.

ASTM D7012-10 (2010). Standard test method for compressive strength and elastic moduli of intact rock core specimens under varying states of stress and temperatures, ASTM International, West Conshohocken, PA, USA.

ASTM D7012-23 (2023). Standard test methods for compressive strength and elastic moduli of intact rock core specimens under varying states of stress and temperatures, ASTM International, West Conshohocken, PA, USA.

Chen, J., Yang, R. and Kang, Y. (2020). Influence of the Rock Length-to-Diameter Ratio and Failure Modes on Uniaxial Compression Strength. Geotech. Geol. Eng., 38, 2551–2557.

Dong, L., Xu, H.F., Fan, P.X. and Wu, Z.C. (2021). On the Experimental Determination of Poisson's Ratio for Intact Rocks and Its Variation as Deformation Develops. Advances in Civil Engineering, Vol. 2021, Article ID 884 3056, 10 pages.

Du, K., Su, R., Tao, M., Yang, C., Momeni, A. and Wang, S. (2019). Specimen shape and cross-section effects on the mechanical properties of rocks under uniaxial compressive stress. Bull. Eng. Geol. Environ., 78, 6061–6074.

EN 1997-1:2004/AC:2009 (2009). Eurocode 7 – Geotechnical design – Part 1: General rules. CEN, Brussels, Belgium.

EN 1997-2:2007 (2007). Eurocode 7 – Geotechnical design – Part 2: Ground investigation and testing. CEN, Brussels, Belgium.

Gao, M., Liang, Z., Li, Y., Wu, X. and Zhang, M. (2018). End and shape effects of brittle rock under uniaxial compression. Arab. J. Geosci., 11, 614.

Gong, F.,Yan, J., Luo, S. and Li, X.B. (2019). Investigation on the linear energy storage and dissipation laws of rock materials under uniaxial compression. Rock Mech. Rock Eng., 52 (11), 4237-4255.

He, M.M., Pang, F., Wang, H.T., Zhu, J.W. and Chen, Y.S. (2020). Energy dissipation-based method for strength determination of rock under uniaxial compression. Shock and Vibration, 2020, article ID 8865958, 13 p.

Hoek, E. and Brown, E.T. (1980). Underground excavations in rock, revised 1st ed. Inst. Min. Metall., CRC Press, London, 536 p.

Hoskins, J.R. and Horino, F.G. (1968). Effects of end conditions on determining compressive strength of rock samples, report of investigations 7171, U.S. Bureau of mines, 22 p.

Hudson, J.A. and Harrison J.P. (2000). Engineering rock mechanics, an introduction to the principles, 2nd impression. Pergamon, Elsevier Ltd, Oxford, UK, 458 p.

ISRM (Commission on standardization of laboratory and field test) (1978). Suggested methods for determining hardness and abrasiveness of rocks. Int. J. Rock Mech. Min. Sci. & Geomech. Abstr., 15, 89-97.

ISRM (Comission on standardization of laboratory and field test) (1979). Suggested methods for determining the uniaxial compressive strength and deformability of rock materials. Int. J. Rock Mech. Min. Sci. & Geomech. Abstr., 16, 135-140.

ISRM (Commission on standardization of laboratory and field Tests) (1983). Suggested methods for determining the strength of the rock materials in triaxial compression (revised version). Int. J. Rock Mech. Min. Sci. & Geomech. Abstr., 20 (6), 283-290.

ISRM (Commission on testing methods from 1998 onwards) (1999). Draft ISRM suggested method for the complete stress-strain curve for intact rock in uniaxial compression, Int. J. Rock Mech. Min. Sci., 36, 279-289.

ISRM (Commission on testing methods) (2007). The complete ISRM suggested methods for rock characterization, testing and monitoring: 1974-2006 („The blue book"). ISRM, Lisbon, Portugal, 638 p.

Liang, C. Y., Zhang, Q. B., Li, X. and Xin, P. (2016). The effect of specimen shape and strain rate on uniaxial compressive behavior of rock material. Bull. Eng. Geol. Environ., 75, 1669-1681.

Liu, Z., Zhang, C., Zhang, C., Gao, Y., Zhou, H. and Chang, Z. (2019). Deformation and failure characteristics and fracture evolution of cryptocrystalline basalt. J. Rock Mech. Geotech. Eng., 11 (5), 990-1003.

Pells, P.J.N. and Ferry, M.J. (1983). Needless stringency in sample preparation standards for laboratory testing of weak rocks. In: Proceedings of 5th International Congress (ISRM). ISRM, Vol 1983 Pt 1, A 203-A 207.

Podnieks, E.R., Chamberlain, P.G. and Thill, R.E. (1972). Environmental Effects on Rock Properties. In: Basic and Applied Rock Mechanics, Proceedings of Tenth Symposium on Rock Mechanics - The American Institute of Mining, Metallurgical, and Petroleum Engineers (AIME), Chapter 8, 215-241.

Štambuk Cvitanović, N. (2012). Istraživanje utjecaja nepravilnosti oblika intaktnih uzoraka na mehanička svojstva vapnenačke stijene (*Investigation on the effects of intact specimens shape deviations on limestone rock mechanical properties*). PhD Thesis. University of Split, Split, Croatia, 250 p (*in Croatian, English abstract*).

Štambuk Cvitanović, N. and Đukić, P. (2014). System and method for automatic recording of a plurality of measurements and verification of specimens in rock mechanics. US Patent App. 14/304,602.

Štambuk Cvitanović, N., Miščević, P., Vrkljan, I. and Kavur, B. (2015a). Application of response surface methodology to model dependence of strength and deformability of limestone rock on intact specimens shape deviations. In: Proceedings of the 13th ISRM International Congress on Rock Mechanics, Montreal, Canada, May 2015, paper 759.

Štambuk Cvitanović, N., Nikolić, M. and Ibrahimbegović, A. (2015b). Influence of specimen shape deviations on uniaxial compressive strength of limestone and similar rocks. International Journal of Rock Mechanics and Mining Sciences, 80, 357-372.

Taheri, A., Fantidis, Y., Olivares, C.L., Connelly, B.J. and Bastian, T.J. (2016). Experimental study on degradation of mechanical properties of sandstone under different cyclic loadings. Geotech. Testing J., 39 (4), 673-687.

Thuro, K., Plinninger, R.J., Zäh, S. and Schütz S. (2001). Scale effects in rock strength properties, Part 1: Unconfined compressive test and Brazilian test. In: Särkkä, P. and Eloranta, P. (eds.): Rock Mechanics – a Challenge for Society, Proceedings of ISRM Regional Symposium EUROCK 2001 - 2001 Swets & Zeitlinger, Lisse, Netherlands, 169-174, 910 p.

U.S. Department of Transportation (1977). Demonstration project # 42, Highway Quality Assurance – Process Control and Acceptance Plans, Federal Highway Administration, Region 15, Demonstration Projects Division, Arlington, Virginia.

Vaneghi, R.G., Saberhosseini, S.E., Dyskin, A.V., Thoeni, K., Sharifzadeh, M. and Sarmadivaleh, M. (2021). Sources of variability in laboratory rock test results. J. Rock Mech. Geotech. Eng., 13 (5), 985-1001.

Xie, W.-Q., Liu, X.-L., Zhang X.-P., Liu, Q.-S. and Wang, E.-Z. (2024). A review of test methods for uniaxial compressive strength of rocks: Theory, apparatus and data processing. J. Rock Mech. Geotech. Eng. (in press), https://doi.org/10.1016/j.jrmge.2024.05.003

Zhang, Q., Zhu, H., Zhang, L. and Ding, X. (2011). Study of scale effect on intact rock strength using particle flow modeling. International Journal of Rock Mechanics and Mining Sciences, 48 (8), 1320-1328.

Zou, C. and Wong, L.N.Y. (2016). Size and Geometry Effects on the Mechanical Properties of Carrara Marble Under Dynamic Loadings. Rock Mech. Rock Eng., 49, 1695–1708.

SAŽETAK

## Utjecaj tolerancija oblika ispitnoga uzorka na određivanje mehaničkih svojstava i svojstava disipacije energije vapnenačke stijene

Jednoosna tlačna čvrstoća (*UCS*), Youngov modul (*E*) i Poissonov omjer (*v*) intaktne stijene ovise o tolerancijama oblika valjkastoga uzorka (ravnost baza *R*, njihova paralelnost *P* i okomitost na os uzorka *O*). Današnji kriteriji prihvatljivosti uzoraka (dopušteni *R*/*P*/*O*) temelje se na oskudnim istraživačkim podatcima iz 1970-ih koji se uglavnom odnose na *UCS* ne uzimajući u obzir kategoriju čvrstoće stijene (*worst case* scenarij). Također su vrlo striktni i, u nekim slučajevima, upitni za provedbu, zahtijevajući inženjersku prosudbu. Kako bi se povećala pouzdanost i olakšala procjena prihvatljivosti ispitnoga uzorka, ova studija istražuje utjecaj tolerancija oblika na sva svojstva *UCS*/*E*/*v* i povezana svojstva disipacije energije (ukupna, elastična i disipacijska energija) za vapnenac i usporedivu stijenu srednje čvrstoće s *UCS* oko 100 - 150 MPa. Pripremljeno je 90 uzoraka s namjerno izazvanim tolerancijama oblika u širemu rasponu (*R* do 0,5 mm; *P*, *O* do 2°), pri čemu je za precizno i točno određivanje *R*/*P*/*O* razvijena posebna oprema. Uzorci su zatim ispitani pri jednoosnome tlačnom naprezanju uz korištenje više relevantnih postavki mjerenja te su određena sva mehanička svojstva i svojstva disipacije energije. Iz velikoga broja eksperimentalnih rezultata i dodatnih statističkih/numeričkih/energetskih analiza uspostavljeni su pouzdani modeli ponašanja za *UCS*/*E*/*v* ovisnost o *R*/*P*/*O* koji se dalje mogu koristiti za procjenu posljedica tolerancija oblika i prihvatljivosti ispitnoga uzorka. Ako se na ove modele primijene granice prirodne varijabilnosti za 'idealne' uzorke, dobivaju se kritične tolerancije koje umanjuju postojeće zahtjeve (npr. *R* = 0,08 mm umjesto 0,05 mm), a koje se predlažu kao dopunske s ciljem optimizacije procesa ispitivanja za stijene srednje čvrstoće.

**Ključne riječi:**
valjkasti ispitni uzorci stijene, tolerancije oblika, mehanička svojstva, svojstva disipacije energije

## Author's contribution

**Nataša Štambuk Cvitanović (1)** (PhD in civil engineering, Full Professor at the Faculty of Civil Engineering, Architecture and Geodesy, University of Split) gave the original idea, carried out all the preparations and experimental work, processing and interpretation of the results, and provided the manuscript draft. **Boris Kavur (2)** (PhD in mining engineering, Associate Professor at the Faculty of Geotechnical Engineering, University of Zagreb) provided the interpretations of the results related to energy dissipation, assisted in data analysis and presentation and contributed to writing, review and editing. **Ivan Vrkljan (3)** (PhD in civil engineering, Emeritus Professor at the Faculty of Civil Engineering, University of Rijeka) provided investigation resources and contributed to the development of the research methodology and presentation of the results. **Predrag Miščević (4)** (PhD in civil engineering, Full Professor, tenure at the Faculty of Civil Engineering, Architecture and Geodesy, University of Split) was a supervisor, contributing with the determination of engineering limits and the review.
All authors have read and approved the final version of the manuscript.